*Geophys. J. Int.* (2009) **176,** 695–714 doi: 10.1111/j.1365-246X.2008.04025.x



# Separation of coseismic and postseismic gravity changes for the 2004 Sumatra–Andaman earthquake from 4.6 yr of GRACE observations and modelling of the coseismic change by normal-modes summation

Caroline de Linage,[1,2] Luis Rivera,[1] Jacques Hinderer,[1] Jean-Paul Boy,[1,3] Yves Rogister,[1] Sophie Lambotte[4] and Richard Biancale[5]

[1]*EOST-IPGS (*UMR 7516 *CNRS–ULP),* 5, *rue René Descartes,* 67084, *Strasbourg Cedex, France*
[2]*Department of Earth System Science, University of California Irvine, Croul Hall, Irvine,* CA 92697-3100*, USA. E-mail: caroline.delinage@uci.edu*
[3]*NASA Goddard Space Flight Center, Planetary Geodynamics Laboratory, Greenbelt, MD* 20771*, USA*
[4]*Laboratoire de Géologie de l'Ecole Normale Supérieure (UMR* 8538*),* 24 *rue Lhomond,* 75231 *Paris Cedex* 5, *France*
[5]*CNES/GRGS,* 18, *Avenue Edouard Belin,* 31401 *Toulouse Cedex* 9, *France*

Accepted 2008 October 20. Received 2008 October 17; in original form 2008 April 28

## SUMMARY

This paper is devoted to the simultaneous determination of the coseismic and postseismic gravitational changes caused by the great 2004 December 26 Sumatra–Andaman earthquake from the time-variable global gravity fields recovered by the Gravity Recovery And Climate Experiment (GRACE) mission. Furthermore, a complete modelling of the elasto-gravitational response of a self-gravitating, spherically layered, elastic earth model is carried out using a normal-modes summation for comparison with the observed coseismic gravitational change. Special attention is paid to the ocean mass redistribution. Special care is paid during the inversion of the data to avoid contamination of tectonic gravity changes by ocean tidal model errors, seasonal and interannual signals originating from continental hydrology and oceanic circulation as well as contamination of the coseismic gravity change by the postseismic relaxation. We use a 4.6-yr-long time-series of global gravity solutions including 26 months of postseismic data, provided by the Groupe de Recherche en Géodésie Spatiale (GRGS). For comparison, the Release-04 solutions of the Center for Space Research (CSR) are also investigated after a spectral windowing or a Gaussian spatial smoothing. Results are shown both in terms of geoid height changes and gravity variations. Coseismic and postseismic gravitational changes estimated from the different gravity solutions are globally similar, although their spatial extent and amplitude depend on the type of filter used in the processing of GRACE fields. The highest signal-to-noise ratio is found with the GRGS solutions. The postseismic signature has a spectral content closer to the GRACE bandwidth than the coseismic signature and is therefore better detected by GRACE. The coseismic signature consists mainly of a strong gravity decrease east of the Sunda trench, in the Andaman Sea. A gravity increase is also detected at a smaller scale, west of the trench. The model for the coseismic gravity changes agrees well with the coseismic signature estimated from GRACE, regarding the overall shape and orientation, location with respect to the trench and order of magnitude. Coseismic gravity changes are followed by a postseismic relaxation that are well fitted by an increasing exponential function with a mean relaxation time of 0.7 yr. The total postseismic gravity change consists of a large-scale positive anomaly centred above the trench and extending over 15° of latitude along the subduction. After 26 months, the coseismic gravity decrease has been partly compensated by the postseismic relaxation, but a negative anomaly still remains south of Phuket. A dominant gravity increase extends over 15° of latitude west of the trench, being maximal south of the epicentre area. By investigating analyses of two global hydrology models and one ocean general circulation model, we show that our GRACE estimates of the coseismic and postseismic gravitational changes are almost not biased by interannual variations originating from continental hydrology and ocean circulation in the subduction area and in the central part of the Andaman Sea, while they are biased by several $\mu$Gal in the Malay Peninsula.

**Key words:** Satellite geodesy; Seismic cycle; Transient deformation; Time variable gravity; Subduction zone processes; Dynamics: gravity and tectonics.

## 1 INTRODUCTION

The determination of the Earth's gravity field and its temporal variation has been greatly improved in terms of spatial resolution and measurement accuracy during the past decade by the Challenging Mini-satellite Payload (CHAMP) satellite launched in 2000 and by the ongoing Gravity Recovery And Climate Experiment (GRACE) mission launched in 2002 (Tapley *et al.* 2004). Since the CHAMP mission, gravity models can be built from a single satellite mission and have gained in accuracy, due to more precise measurement techniques (Global Positioning System (GPS)-to-satellite and/or satellite-to-satellite trackings) and lower satellite altitudes. For example, the accuracy of the GRACE-derived model EIGEN-GRACE02S is 1 cm at a half-wavelength resolution of 275 km and less than 1 mm at 1000 km (Reigber *et al.* 2005). Moreover, the GRACE mission allows one to build time-variable gravity models at monthly intervals. The theoretical resolution ranges from 400 to 40 000 km (Tapley *et al.* 2004), but water mass variations can reliably be estimated only up to a half-wavelength resolution of about 750 km with an accuracy smaller than 5 cm (Schmidt *et al.* 2006; Wahr *et al.* 2006) of equivalent water height, equivalent to less than 1 mm of geoid height.

Therefore, variations from various geophysical sources can be detected. Since the aim of GRACE is to provide the seasonal-to-interannual evolution of hydrosphere, cryosphere and ocean circulation, the contributions from well-known geophysical sources are removed by using geophysical models: solid Earth, ocean and pole tides, non-tidal high-frequency atmospheric variations and the subsequent response of an ocean model to the atmospheric surface pressure variations and winds (Bettadpur 2007; Flechtner 2007).

In addition, as already demonstrated by Mikhailov *et al.* (2004) and Sun & Okubo (2004a), earthquakes with magnitude larger than 7.5 can be detected by GRACE as their signature can be two orders of magnitude larger than the GRACE errors. However, the GRACE limited spatial resolution prevents the restitution of the full signature of such events (Sun & Okubo 2004b). The 2004 December 26 Sumatra–Andaman earthquake is one of the biggest earthquakes ever recorded and the biggest one that occurred during the GRACE mission. Estimates of its magnitude range between 9.1 (Ammon *et al.* 2005) and 9.3 (Stein & Okal 2005). The area of the rupture surface is about $1200 \times 200$ km, spreading from northwest of Sumatra to the Andaman Islands (Ammon *et al.* 2005).

Several studies of the gravity signature of the Sumatra–Andaman earthquake in the GRACE observations have already been published; they are listed in Table 1. Particular care is needed to separate the earthquake signature from the hydrological signals that are not negligible near continental areas, particularly in the monsoon zone (Tapley *et al.* 2004; Wahr *et al.* 2004; Frappart *et al.* 2006). The annual hydrological variations can be removed by computing the difference between the solutions obtained before and after the earthquake, the time interval between the solutions being an integer number of years (Han *et al.* 2006; Chen *et al.* 2007; Panet *et al.* 2007). The signal-to-noise ratio is enhanced by stacking the differences over 1 month (Panet *et al.* 2007), 6 months (Han *et al.* 2006) or 21 months (Chen *et al.* 2007). However, because of the stacking method, the postseismic signal contaminates the estimate of the coseismic signal. Postseismic effects are expected to be large for such a big earthquake. Their timescale ranges from days to years. For example, the timescales of afterslip and poroelastic rebound range from days to months and viscoelastic relaxation lasts for years (Freymueller *et al.* 2000). Since interannual hydrological variations are not removed by a stacking method, they can be removed from the GRACE observations by using a global hydrological model (Panet *et al.* 2007). However, the difference in the spatial resolution between GRACE and the model leaves an annual residual signal. Ogawa & Heki (2007) simultaneously estimate both effects by fitting to the geoid height time-series the annual and semi-annual signals, a coseismic jump and a postseismic relaxation. They find a strong dominant negative gravity anomaly in the Andaman Sea followed by a slow postseismic rebound estimated over 22 months after the earthquake. Global gravity solutions are used by Panet *et al.* (2007), Ogawa & Heki (2007) and Chen *et al.* (2007) whereas solutions from a regional inversion are used by Han *et al.* (2006). Panet *et al.* (2007) perform a continuous wavelet analysis of the geoid time-series which allows them to separate large and small spatial scales. They find a short-term postseismic effect located in the Andaman Sea and a large-scale effect still ongoing 9 months after the earthquake. More recently, Han & Simons (2008) have used a spatiospectral localization technique to extract the coseismic jump from the harmonic coefficients. This enhances the spatial resolution of the harmonic solutions to a level comparable to that of the regional inversion (about 500 km). However, they did not address any postseismic effects.

Some authors (Han *et al.* 2006; Ogawa & Heki 2007) model the coseismic effect by computing the gravity effect of a rectangular finite fault buried in an elastic homogeneous half-space. Density discontinuities are introduced in the model in a second step. The effect of surface deformation alone does not explain the gravity observations. Dilatation in the crust has also a significant effect. Other authors (Panet *et al.* 2007) consider a self-gravitating, spherically layered, elastic earth model. They find a strong negative gravity anomaly in the Andaman Sea. However, the computation of the gravity effect is not explained in detail.

In this study, we estimate the earthquake signature from 4.6-yr-long time-series of GRACE global gravity field solutions from different processing centres (Toulouse Team of Space Geodesy versus Center for Space Research; CSR) and check the impact of filtering using different filters (spectral low-pass filter versus the classical Gaussian filter). We show that it is very important to carefully separate the postseismic effect from the coseismic one to avoid a mixing of both effects as it is the case for example in Chen *et al.* (2007). This separation is possible thanks to a 26-month-long postseismic time-series. Simultaneously to estimating the seismic signatures in the spatial domain, we estimate the seasonal gravity changes due to continental hydrology and oceanic circulation. The postseismic effect is thus estimated over two complete annual cycles after the earthquake which avoids the postseismic estimate being biased by annual hydrological variations. The aliasing errors of the $S_2$ tidal wave are also inverted from the GRACE fields. In addition, the impact of the interannual variations in continental hydrology and oceanic circulation on our estimates of the seismic signatures is investigated from analyses of global models. Finally, on the contrary to the previous studies of Han *et al.* (2006) and Ogawa & Heki (2007), we favour a global approach in the modelling of the coseismic effect by using a self-gravitating, stratified, spherically symmetric, elastic earth model and a detailed model of the seismic source. In particular, we compute the gravitational effect of the ocean mass static redistribution after the earthquake, which has not been dealt with in previous studies.

**Table 1.** Comparison of the present work to previous studies.

| | Han *et al.* (2006) | Panet *et al.* (2007) | Ogawa & Heki (2007) | Chen *et al.* (2007) | Present work | |
|---|---|---|---|---|---|---|
| Type of data | Regional inversion | Global inversion (Stokes coefficients = Level-2 products) | | | | |
| Processing centre | OSU | GRGS | CSR-RL01 | CSR-RL04 | GRGS | CSR-RL04 |
| Filtering | None | Spectral constraint towards the static field over $\ell = 30–50$ + wavelet analysis | 350-km Gaussian smoothing | Decorrelation filtering + 300-km Gaussian smoothing | Spectral constraint towards the static field over $\ell = 30–50$ | Spectral windowing with a cosine taper over $\ell = 30–50$ + 350-km Gaussian smoothing |
| Quantity shown | Gravity | Geoid | Geoid | Equivalent water height | Geoid and gravity | |
| Data length | 2.3 yr 02/2003–06/2005 | 3.1 yr 08/2002–09/2005 | 4.6 yr 04/2002–10/2006 | 3.8 yr 01/2003–09/2006 | 4.6 yr 08/2002–02/2007 | 4.6 yr 08/2002–02/2007 |
| Coseismic estimation in GRACE | Stacking of 1- and 2-yr differences: (2005 – 2004) + (2005 – 2003) | Stacking of 1-yr differences: Jan 2005 – Jan 2004 | Least-squares fit to the time-series | Stacking of 2-yr differences: (2005 + 2006) – (2003 + 2004) | Least-squares fit to the time-series | |
| Contamination by postseismic (length) | Yes (6 months) | Weak (1 month) | None | Yes (21 months) | None | |
| Postseismic estimation in GRACE | None | Time-variable wavelet analysis over 8 months | Fit of an exponential relaxation over 22 months | Only at two points | Fit of an exponential relaxation over 26 months | |
| Coseismic modelling | Dislocation in a homogeneous half-space | Normal-modes summation in a SNREI earth model + half-space 2-D flat model of the lithosphere | Dislocation in a homogeneous half-space | None | Normal-modes summation in an SNREI earth model | |
| Ocean response | None | None | None | None | Yes | |

OSU: Ohio State University, Columbus, USA.
GRGS: Groupement de Recherche en Géodésie Spatiale at Centre National d'Etudes Spatiales, Toulouse, France.
CSR: Center for Space Research at University of Texas, Austin, USA.

## 2 ESTIMATION OF EARTHQUAKE SIGNATURE IN GRACE GRAVITY SOLUTIONS

### 2.1 Methodology

We use the global gravity solutions of the CNES/Groupe de Recherche en Géodésie Spatiale (GRGS) (Biancale *et al.* 2008) available as a time-series of harmonic coefficients of the gravitational potential. A complete description of the processing strategy and models used is given by Lemoine *et al.* (2007). The degree-two and order-zero coefficient $C_{20}$ mainly comes from LAGEOS-1/2 SLR data. The remaining information comes from GPS-to-satellite and satellite-to-satellite tracking data. Each set of coefficients is computed every 10 d over a 30-d period, with a double weight given to the central 10 d in the inversion. The inversion is made up to harmonic degree 50. The harmonic coefficients higher than 30 are gradually constrained to the coefficients of the static field EIGEN-GL04S (Biancale *et al.* 2008) so that no more information comes from the data at degree 50. This strategy allows one to keep some of the high-frequency variability without being too much contaminated by the noise. Thus, inconvenient north–south stripes are significantly attenuated and no additional filtering is applied to the solutions. The spatial resolution is approximately 666 km.

For a given time, we compute over a $1^\circ \times 1^\circ$ grid on a sphere of radius $a = 6378$ km, the geoid height variation $\Delta N$, proportional to the difference $\Delta\Phi$ between the geopotential at a given time and the reference geopotential EIGEN-GL04S:

$$\Delta N(a,\theta,\phi) = \frac{\Delta\Phi(a,\theta,\phi)}{g_0(a)} = a\sum_{\ell m}\left[\Delta\overline{C}_{\ell m}\overline{Y}^c_{\ell m}(\theta,\phi) + \Delta\overline{S}_{\ell m}\overline{Y}^s_{\ell m}(\theta,\phi)\right], \quad (1)$$

where $g_0(a) = GM/a^2$, $\overline{Y}^c_{\ell m}(\theta,\phi)$ and $\overline{Y}^s_{\ell m}(\theta,\phi)$ are the real fully normalized spherical harmonics of harmonic degree $\ell$ and azimuthal order $m$. $\overline{C}_{\ell m}$ and $\overline{S}_{\ell m}$ are the Stokes coefficients. The gravity disturbance $\Delta g$, which is the radial derivative of the geopotential variation, is given by

$$\Delta g(a,\theta,\phi) = g_0(a)\sum_{\ell m}(\ell+1) \times\left[\Delta\overline{C}_{\ell m}\overline{Y}^c_{\ell m}(\theta,\phi) + \Delta\overline{S}_{\ell m}\overline{Y}^s_{\ell m}(\theta,\phi)\right]. \quad (2)$$

$\Delta N$ and $\Delta g$ contain the same information through the Stokes coefficients. Nevertheless, we compute both quantities: $\Delta N$ will mainly reflect the large wavelengths of the gravitational effect whereas $\Delta g$ will be more sensitive to the small ones because of the $(\ell + 1)$ term in eq. (2).

We use a series of 153 monthly solutions spanning 4.6 yr, from 2002 July 29 to 2007 February 22. The series consists of 77 solutions prior to and 76 solutions posterior to the earthquake, spanning 29 months (2002 July 29 –2004 December 24) and 26 months (2005 January 4–2007 February 22), respectively. There are three gaps of respectively 70, 20 and 30 d, occurring between 2002 December and 2003 February, in 2003 June and between 2004 December and 2005 January. The last gap is due to the rejection of the solutions that include the earthquake date (2004 December 26). The trade-off between the annual hydrological cycle and the postseismic relaxation is reduced because we have restricted the postseismic period to two complete annual cycles.

As shown by the time-series in Fig. 1, the variability of the GRACE residues can be of the same order as the coseismic effect of the Sumatra–Andaman earthquake and the signal-to-noise ratio is higher for the gravity than for the geoid. One of the sources of this variability is hydrology in Southeast Asia that undergoes one of the strongest hydrological cycles in the world with high precipitation during the monsoon period. The closest hydrological basin in the studied area is the Mekong basin sprawling over Thailand and Cambodia (Frappart *et al.* 2006). Large signals in GRACE also come from the Brahmaputra and Ganges basins (Wahr *et al.* 2004). The biggest effects on the geoid and on the gravity are located on the continents but significant annual signals can be found even offshore, for example, in the Andaman Sea. The limited spatial resolution of GRACE indeed produces a leakage of the continental signal towards the oceans. For example, the annual amplitude is 2.2 mm for the geoid variation and only 0.5 μGal for the gravity variation at point B (centre panels of Fig. 1). The maximal amplitude of the geoid variation is reached at the end of October and is followed by a strong decrease during the last months of the year, which coincides with the occurrence of the earthquake.

Another source of variability in the GRACE residues are the seasonal and interannual changes in the ocean circulation. These variations are smaller than those due to hydrology and their amplitude is often at the noise level.

Besides, the models used for de-aliasing the GRACE raw data introduce errors at long periods in the final solutions. This is the case of the ocean tide models (Ray & Luthcke 2006). Model errors of the $S_2$ tidal wave produce an alias at 161-d period that is clearly visible in the Andaman Sea, particularly at point B (bottom centre panel of Fig. 1) where its amplitude is larger than those of the annual and semi-annual signals. It is therefore easy to remove this alias from the GRACE time-series. Ignoring it may bias the estimate of the coseismic effect when computing the gravity variations at 1-yr intervals.

Finally, there is an obvious postseismic signal consisting in a gravity increase, especially at points C and D located near the Sunda trench (Fig. 1). The velocity of the process decreases with time. It is almost null 26 months after the earthquake. Such a postseismic gravity change can be explained by several physical processes such as poroelastic rebound (Peltzer *et al.* 1998) as invoked by Ogawa & Heki (2007), frictional deformation, generally named afterslip, and ductile deformation in the lower crust or upper mantle (Freymueller *et al.* 2000). All of these processes are responsible for postseismic creep. Time dependence of the phenomenon hinges on the rheology of the creeping region (Montesi 2004): ground displacements caused by afterslip are generally modelled by a logarithmic function of time, while those due to viscous flow are characterized by an increasing exponential function. The timescales of these processes range from several weeks for afterslip to several years for viscous relaxation of the mantle. Since the duration of the observed postseismic signal is generally larger than 6 months, we favoured the exponential relaxation law. But, the duration of the signal being shorter than 26 months, only a limited range of time constants can be assessed with reliability. Moreover, the GRACE temporal resolution is not high enough to deduce time constants smaller than 1 month.

From these considerations, it results that the difference between the gravity solutions for 2005 January and 2004 December is not a good estimate of the coseismic effect because of the strong hydrological gradient occurring at the earthquake time. Similarly, stacking over several months the differences between two solutions at a 1-yr interval does not provide a good estimate of the postseismic effect.

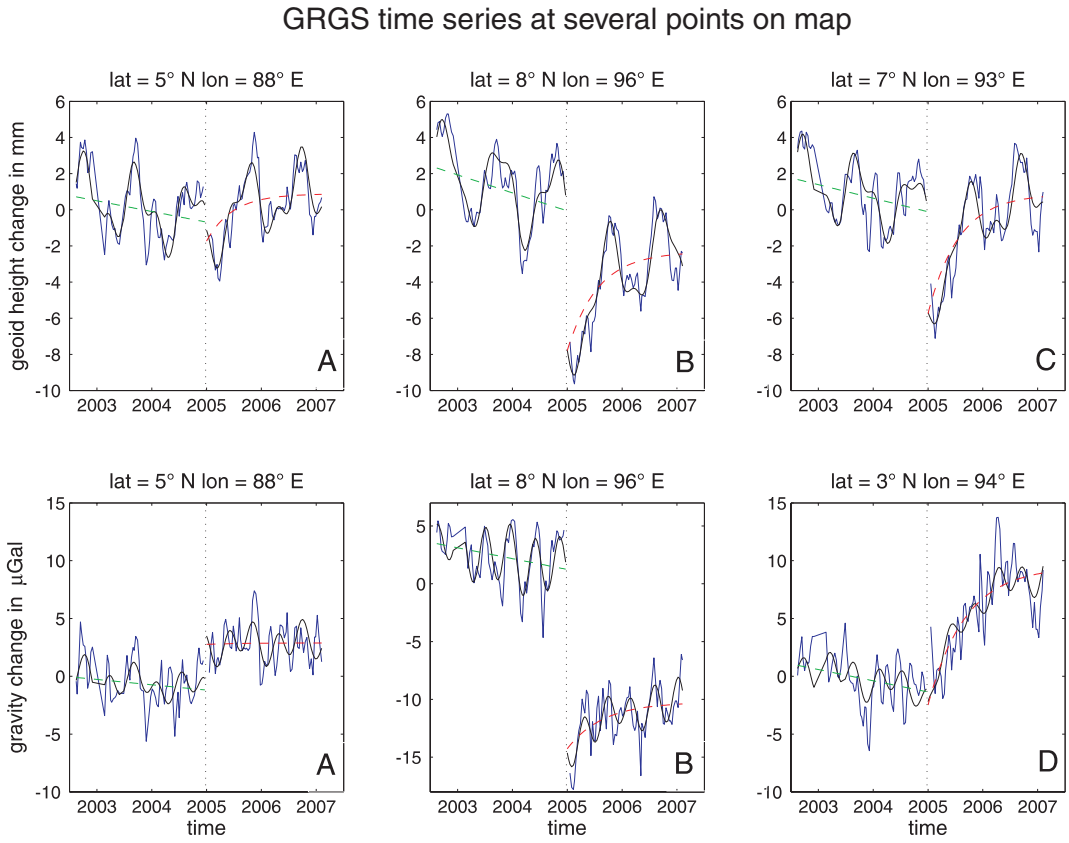


**Figure 1.** Time-series of geoid height (top panels) and gravity (bottom panels) variations estimated from the GRACE 10-d global gravity solutions of the GRGS (blue curve), total fitted signal by non-linear inversion (black curve), fitted linear trend before the earthquake (green line) and fitted postseismic exponential relaxation (red curve). Letters refer to locations plotted in Figs 2, 4, 6 and 10.

To separate the above-mentioned effects in the GRACE data, we adopt the following strategy. At each point of a $1^\circ \times 1^\circ$ grid, we simultaneously fit to the geoid and gravity time-series the following time-function:

$$y(t) = \sum_{i=1}^{3} a_i \cos(\omega_i t + \phi_i) + \begin{cases} b\,t + c_1 & \text{before the earthquake} \\ c_2 + d\,(1 - \mathrm{e}^{-t/\tau}) & \text{after the earthquake,} \end{cases} \quad (3)$$

where $t$ is the time interval with respect to earthquake origin time and model parameters are:

(1) $a_1, \phi_1, a_2, \phi_2$ are the amplitudes and phases of the annual and semi-annual waves to model the seasonal and annual variations of hydrology and long-period oceanic circulation;
(2) $a_3$ and $\phi_3$ are the amplitude and phase of a 161-d sine curve to correct the errors on the $S_2$ tidal wave;
(3) $b$ is a linear trend before the earthquake;
(4) $c_2 - c_1$ is the coseismic jump;
(5) $\tau$ and $d$ are the relaxation time and total postseismic gravity change reached at the end of the relaxation.

We do not take into account the effect of the 2005 March 28 Nias earthquake because its amplitude in the gravity field is negligible compared to that of the 2004 December 26 earthquake as shown by Panet *et al.* (2007).

We compute the 11 parameters by a non-linear least-squares minimization using a quasi-Newton iterative algorithm (Tarantola 2005). We introduce *a priori* information (mean and variance) on each parameter. No spatial correlation is introduced. We also take the errors on the data into account. The spatial distribution of the errors of the GRACE gravity solutions is purely zonal, with higher errors at the equator than at the poles (Wahr *et al.* 2006). For the GRGS solutions, the calibrated one-sigma errors at the equator are 0.6 mm for the geoid height and 2.5 µGal for the gravity (Lemoine, personal communication, 2007). These calibrated errors are however quite optimistic.

For comparison with the GRGS solutions, we also investigate the CSR-RL04 global monthly solutions expanded up to degree 60 (Bettadpur 2007) over the same period from 2002 August to 2007 February, the 2004 December solution being excluded. We also replace the $C_{20}$ coefficients by the more accurate estimates from the analysis of SLR data of five geodetic satellites (Cheng & Tapley 2004). Since the CSR gravity fields are not forced to follow the static field, we have to find the appropriate filtering for the CSR solutions for the fairest comparison with the GRGS solutions. We first apply an isotropic Gaussian filter of radius 350 km. However, it reduces energy even at small degrees ($-3$ dB at $\ell = 18$). A low-pass filter in the spectral domain, which preserves the small degrees and removes the highest ones, is more appropriate. Since the constraint begins to act on the GRGS fields from degree 30, we preserve the degrees smaller than 30 in the CSR fields and filter the others with a cosine taper decreasing from one at $\ell = 30$ to zero at $\ell = 50$. However, there is still a lot of noise at $\ell = 30$–$40$ after such a filtering. So, the solutions are noisier after a spectral windowing with a cosine taper over degrees 30–50 than after a 350-km Gaussian smoothing.

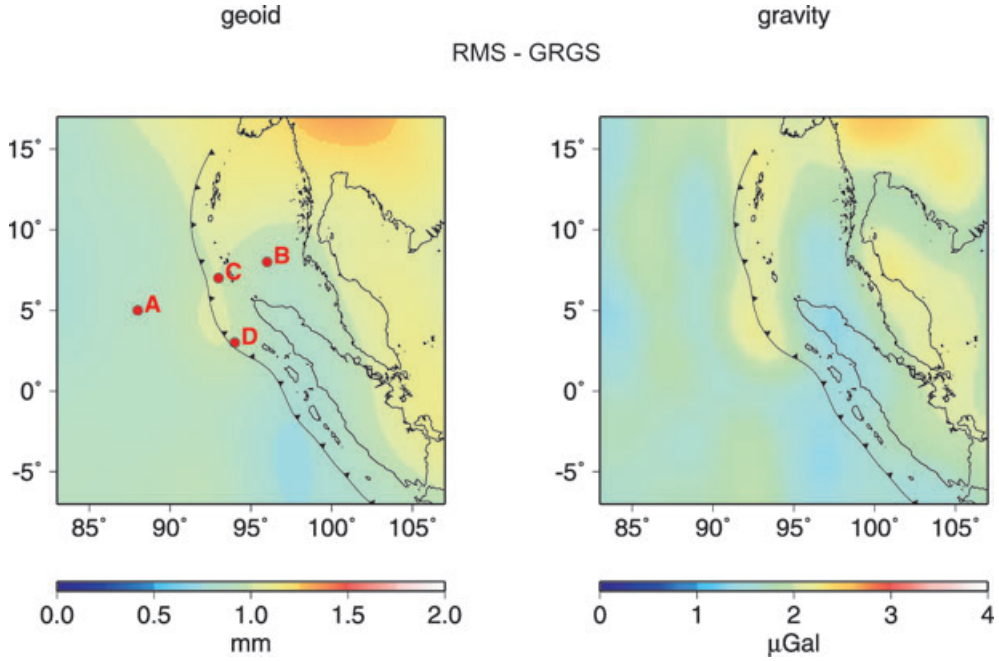


**Figure 2.** The rms of the residues of geoid height (left-hand panel) and gravity (right-hand panel) after inversion of the GRACE-GRGS gravity solutions. Red dots and associated letters refer to the locations where time-series of Fig. 1 are plotted. The Sunda trench contour after Gudmundsson & Sambridge (1998) is superimposed, indicating the subduction of the Indian and Australian Plates beneath the Sunda Shelf.

### 2.2 Results

Results of the inversion are displayed over a 24° × 24° area with an interpolation between each point of a 1° × 1° grid. The Sunda trench is also plotted after Gudmundsson & Sambridge (1998), indicating the subduction of the Indian and Australian Plates beneath the Sunda Shelf. The rms of the residues are shown in Fig. 2 for the GRGS solutions. The mean rms over the area is 1 mm for the geoid and 1.8 µGal for the gravity. The largest rms are found at places where the hydrological and oceanic signals are the strongest, such as Myanmar, Thailand and Cambodia, as well as in the Gulf of Thailand. They are due to unmodelled non-periodic variations. The rms larger than 2 µGal are found over the Sunda trench, from north of Sumatra to the Andaman Islands.

For the geoid, the mean rms is of the same order of magnitude for every solution but is much larger for the gravity with the CSR solutions, that is 2.1 µGal for the Gaussian filtered solutions and 4.2 µGal for the spectrally filtered ones. The latter have in addition the slowest convergence speed among the three solutions. Moreover, the spatial distribution of the rms is disturbed by north–south stripes in the CSR solutions which is not the case in the GRGS ones. The signal-to-noise ratio is therefore higher for the GRGS solutions and lower for the CSR spectrally filtered solutions. That is why we will show in detail the results obtained from the GRGS solutions and take them as a reference in the following discussion.

The parameters are generally well constrained by the data and moderately depend on the *a priori* variance, except for the relaxation constant. This will be discussed in Section 2.2.3

#### *2.2.1 Ocean tide model errors*

Aliasing is due to errors of the ocean tide model FES-2004 (Lyard *et al.* 2006) on the $S_2$ tidal wave for both the GRGS and CSR solutions. Fig. 3 shows the amplitude of the corresponding gravity variation for the GRGS solutions. We find large amplitudes in the

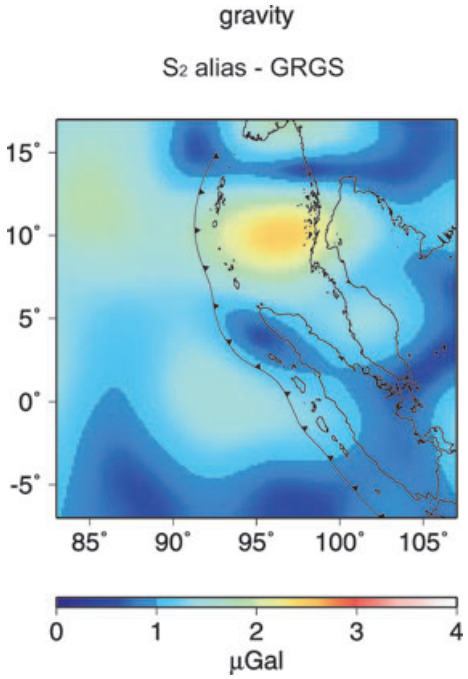


**Figure 3.** Amplitude of the aliasing due to the $S_2$ ocean tidal wave in the GRACE-GRGS solutions.

Andaman Sea reaching 2.5 µGal. This may be equivalent to a maximal error of 58 mm on the $S_2$ predicted height in that area. At point B (bottom centre panel of Fig. 1), aliasing is four times larger (2.0 µGal) than the annual and semi-annual signals. Because of the high amplitude of the aliasing of $S_2$, its modelling strongly reduces the rms in the Andaman Sea and reduces the contamination of the coseismic and postseismic effects.

### 2.2.2 Coseismic signature

*GRGS solutions*

Our estimate of the coseismic signature of the 2004 Sumatra-Andaman earthquake in the GRGS gravity solutions is shown by Fig. 4 and the corresponding one-sigma error is displayed in Fig. 5. For both the geoid and gravity, the mean over the area is negative. The complete signature consists of a strong negative anomaly in the Andaman Sea and a weak positive one west of the subduction trench. Both anomalies are well separated by the trench and the iso-value contour lines are remarkably parallel to the trench over more than 10° of latitude. Regarding the geoid variation, the anomalies spread at larger scale than for the gravity because the former is more sensitive to large scales than the latter. The positive anomaly spreads over a larger area than the negative one. The peak-to-peak amplitude is 7 mm for the geoid and 20 μGal for the gravity. The maximum of the negative anomaly is −8.0 mm for the geoid and −16 μGal for the gravity; it is located at 8°N–97°E for the geoid and westwards for the gravity, at 96°E (point B). Maximum values of the geoid are negative, around −1 mm so that there is no uplift of the geoid. The maximum positive part of the gravity variation is +4 μGal; it is located at 5°N–88°E (point A). A smaller positive anomaly reaching +2 μGal is located close to the equator, over the trench.

The negative anomaly of the gravity variation does not leak north-eastwards, indicating that there is no contamination with hydrology in Myanmar, Cambodia and Thailand. The main geophysical effects other than the earthquake have been consequently removed by our fit without any additional filtering.

The *a posteriori* one-sigma mean errors on the coseismic jump are 0.5 mm for the geoid and 1.5 μGal for the gravity. In the subduction zone as well as in the Andaman Sea, it is constant around 0.6 mm. For the gravity, however, the error is larger between the Nicobar and Andaman Islands and south of the epicentre reaching 2 μGal. It is smaller in the Andaman Sea, around 1.5 μGal. These calibrated errors are, however, quite optimistic. In comparison, the rms of the post-fit residues of Fig. 2 are indeed larger, particularly for the geoid.

*RL04-CSR solutions*

The estimate of the coseismic signature in the CSR gravity solutions is shown by Figs 4(b) and (c) for the two filterings that have been tested, which are the spectral windowing with a cosine taper and the spatial Gaussian filtering, respectively. The amplitudes of the geoid and gravity variations are respectively 30 and 50 per cent smaller with the Gaussian filter. This is due to the fact that this filter acts on every spatial wavelength whereas the spectral filter dampens the half-wavelengths smaller than 666 km. Peak-to-peak differences after the spectral windowing and the Gaussian filtering are respectively 8 and 5.5 mm for the geoid and 28 and 14 μGal for the gravity. Amplitudes found with the CSR solutions after a spectral filtering are similar to those obtained with the GRGS solutions for the geoid but are 40 per cent larger for the gravity. However, the location of the anomalies with respect to the trench is very similar for both solutions. Although two positive anomalies are found again with the CSR solutions, the longitudinal extent of the northern one is smaller in the CSR solutions. Moreover, the amplitude of the southern anomaly is larger than that of the northern one on the contrary to the results with the GRGS solutions. Finally, there is a negative anomaly over Thailand in the CSR solutions that may be due to uncorrected hydrological changes in the Chao Phraya basin. Such an anomaly is, however, not found in the GRGS solutions.

### 2.2.3 Postseismic signature

*GRGS solutions*

Total postseismic gravity change $d$ and relaxation time $\tau$ that both characterize the postseismic response are displayed in Fig. 6 for the GRGS solutions. Since $\tau$ does not exceed 0.85 yr (i.e. 10 months), the postseismic gravity change after 26 months is very close to the total postseismic gravity change. For both the geoid and the gravity, $d$ (shown by Fig. 6a) is a positive 'banana-shaped' anomaly spreading over 15° of latitude along the rupture zone and following the direction and curvature of the trench, from south of the epicentere area to north of the Andaman Islands. Once again, the signature on the geoid contains larger wavelengths than the signature on the gravity. For the geoid, it is positive everywhere on the area whereas for the gravity it rapidly decreases to negative values at the western and eastern edges, especially at the western edge. The gradient at these locations is remarkably perpendicular to the trench. For the geoid, the maximum of $d$ is 6.8 ± 0.3 mm in the vicinity of the Nicobar Islands, at 7°N–93°E (point C). For the gravity, the maximum value of 12.3 ± 1.2 μGal is located at 3°N–94°E (point D), near the epicentre. On both sides of the positive anomaly, there are two negative anomalies that reach respectively −4.2 ± 1.2 μGal in the Indian Ocean and −0.4 ± 1.2 μGal at 7°N–99°E, south of Phuket. *A posteriori* errors on $d$ are about 0.3 mm for the geoid and 1.2 μGal for the gravity all over the area.

The relaxation constant $\tau$ is shown in Fig. 6(b). If a loose constraint is applied to $\tau$, it takes unrealistic values. So, we impose a tight constraint on it: we take 0.7 yr (i.e. about 8.5 months) for *a priori* mean value, which is the third of the postseismic period, and 0.2 yr for its variance. For the gravity, the mean value of $\tau$ is the *a priori* value. But there are areas where $\tau$ departs from it. For the geoid, however, the mean value of $\tau$ is 0.6 yr which is smaller than the *a priori* value. Ogawa & Heki (2007) found the same value. We distinguish three zones both in geoid and gravity: in the area of the Andaman and Nicobar Islands and in the north of the Andaman Sea, $\tau$ is small (around 0.4–0.5 yr); then in the northern part of Sumatra, it is larger (around 0.7–0.8 yr) and finally, south of the epicentre area, it is small (around 0.4–0.5 yr) again. Small values of $\tau$ are correlated with large errors on the coseismic jump which indicates a trade-off between both parameters. Errors on $\tau$ are shown in Fig. 7. For both the geoid and the gravity, they are smaller over the area of positive postseismic gravity change: they reach minima of about 0.06 yr (25 d) for the geoid and 0.13 yr (50 d) for the gravity in the area between the Andaman and Nicobar Islands. This means that an exponential relaxation law fits the data rather well in that area, in particular for the geoid (i.e. at large scales). Elsewhere, the errors take the *a priori* value indicating the lack of information.

Large values of $d$ and $\tau$ are found in Myanmar, Thailand, Cambodia and Vietnam: they might be due to a positive interannual water mass balance over these areas.

*RL04-CSR solutions*

The postseismic signature estimated from the CSR solutions after applying a spectral windowing (resp. a 350-km Gaussian filter) is displayed in Fig. 8 (resp. Fig. 9). As for the coseismic signature, the difference due to the filtering leads to smaller amplitudes of the geoid (resp. gravity) variations of about 30 per cent (resp. 50 per cent) with the Gaussian filter. Amplitudes found with the CSR solutions after a spectral windowing are smaller than those obtained with the GRGS solutions for the geoid but are larger for the gravity. On the contrary to the result with the GRGS solutions, the positive anomaly obtained with the CSR solutions does not follow the curvature of the subduction and its direction is quasi-north–south. The

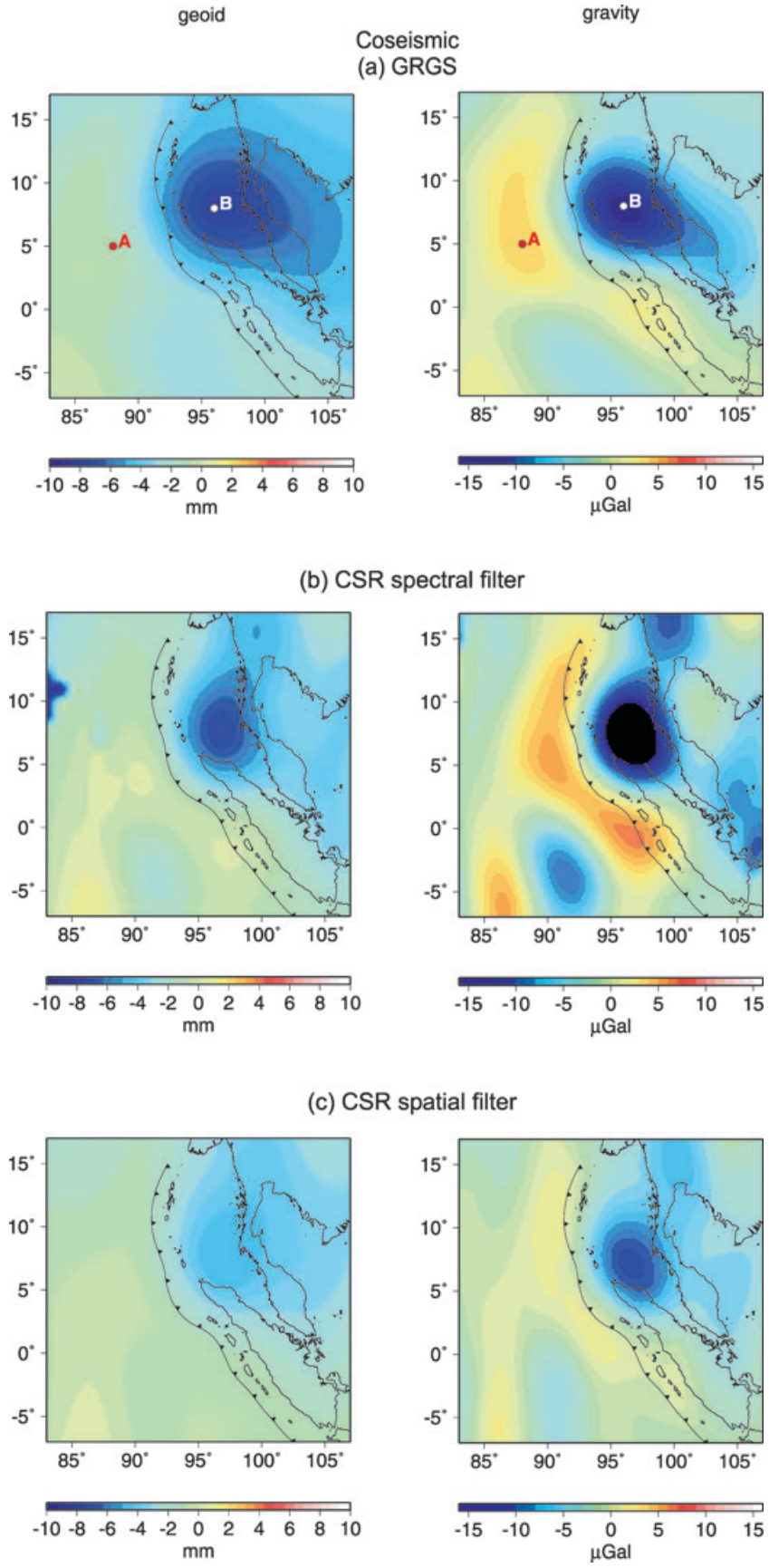


**Figure 4.** Coseismic jump affecting the geoid (left-hand panels) and the gravity (right-hand panels) estimated from the GRACE gravity fields of GRGS (a) and CSR after a spectral filtering with a cosine taper over degrees $\ell = 30$–$50$ (b) or a smoothing with a 350-km Gaussian filter (c). White and red dots and associated letters indicate the locations where time-series of Fig. 1 are plotted.

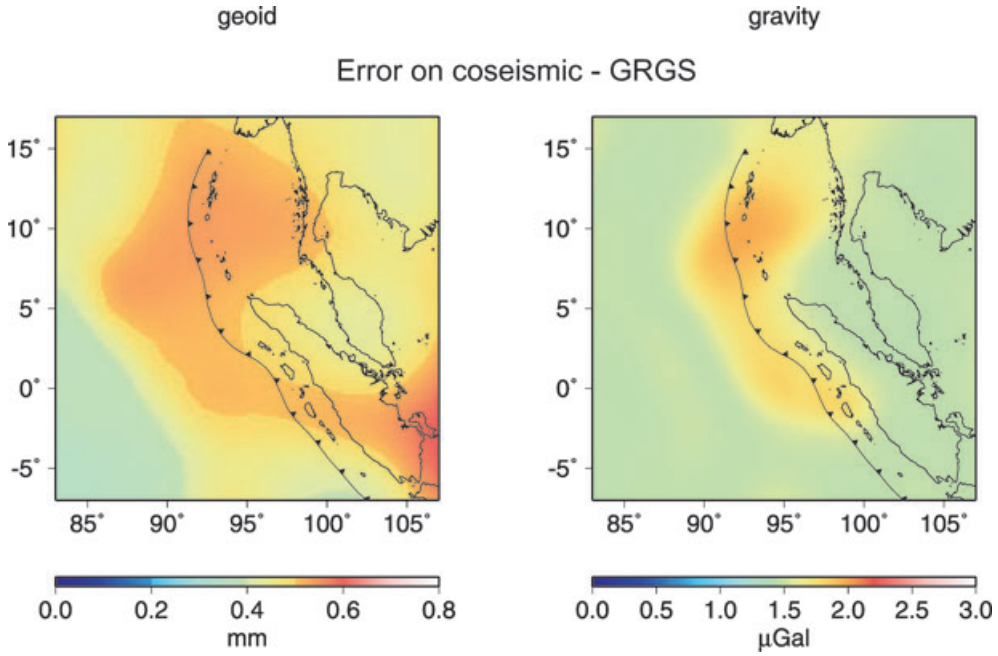


**Figure 5.** *A posteriori* error on the coseismic jump affecting the geoid (left-hand panel) and the gravity (right-hand panel) from the GRGS solutions.

pattern of $\tau$ for the solutions filtered with the spectral windowing is very noisy for both the geoid and the gravity, with north–south stripes that prevent from any interpretation. As for the solutions filtered with the Gaussian filter, $\tau$ is quasi-constant over the entire area, indicating that no information on $\tau$ comes from these data.

#### *2.2.4 Permanent effect 26 months after earthquake*

Fig. 10 shows the sum of the coseismic effect and postseismic relaxation estimated 26 months after the earthquake for each of the three solutions.

In the GRGS solutions (Fig. 10a), the permanent signature is still bipolar like the coseismic one, but the positive and negative anomalies are now symmetric in amplitude and the orientation of the dipole has rotated counter-clockwise being now NW–SE. The positive anomaly is again more stretched than the negative one. The extrema are 3.1/−3.3 mm for the geoid, and 12.3/−13.6 µGal for the gravity. Peak-to-peak amplitudes are 6.4 mm for the geoid and 26 µGal for the gravity. The location of the anomalies is different from the coseismic signature: the negative anomaly is slightly shifted to the southeast, south of Phuket, at 7°N–98°E where postseismic relaxation is negative, and the positive anomaly lies further southeastwards, at 1°N–96°E, south of the epicentre where postseismic relaxation is the largest.

The permanent signatures estimated from the CSR solutions after applying a spectral windowing and a 350-km Gaussian filter are shown in Figs 10(b) and (c), respectively. The difference in filtering leads to a peak-to-peak amplitude that is 50 per cent smaller with the Gaussian filter than that obtained with the spectral windowing. The spatial pattern is however similar. The maximum of the positive anomaly is shifted to the northwest with respect to that of the GRGS solutions, leading to a more longitudinal orientation. The peak-to-peak amplitude found with the spectral windowing is 50 and 30 per cent larger for the gravity and geoid, respectively. The order of magnitude of the signature obtained with the GRGS solutions agrees better with that obtained with the Gaussian-filtered CSR solutions.

## 3 MODELLING OF THE IMPACT OF GLOBAL HYDROLOGY AND OCEANIC CIRCULATION

Continental hydrology and oceanic circulation are two sources of errors when estimating the coseismic and postseismic signatures from the GRACE solutions. Interannual variations in the oceanic circulation and even in continental hydrology (because of the proximity of the monsoon zone) may have been absorbed in the estimated coseismic jump and/or in the estimated postseismic relaxation. We compute the gravity changes from the combined predictions of the water content in the soil as well as the snow cover over the continents, and those of the non-tidal and baroclinic pressure variations at the ocean bottom. The predictions are converted into a surface mass load at the Earth's surface. Then, we compute the gravity change as seen by GRACE. We use the 3-hr analyses of the Global Land Data Assimilation System (GLDAS) hydrology model (Rodell *et al.* 2004) as well as the 6-hr analyses of the European Center for Medium-range Weather Forecasts (ECMWF) operational model (Viterbo & Beljaars 1995). Regarding the global oceanic circulation, we investigate the 12-hr bottom pressure analyses of the Estimating the Circulation and Climate of the Ocean (ECCO)/JPL model (Stammer *et al.* 2002). The investigated period is the same as for the GRACE gravity data, from 2002 July 29 to 2007 February 22. The predictions are transformed into 10-d means. A running average is applied to three consecutive 10-d predictions with weights 0.5/1/0.5, as the GRACE-GRGS gravity fields were built. To work at the same spatial resolution as GRACE, they are low-pass filtered with a cosine taper decreasing from one at $\ell = 30$ to zero at $\ell = 50$. We fit to both combinations (ECMWF + ECCO and GLDAS + ECCO) the same parameters as for the GRACE data, except the 161-d sine curve. Consequently, the resulting coseismic jump and total postseismic effect stand for the biases of our inversion method

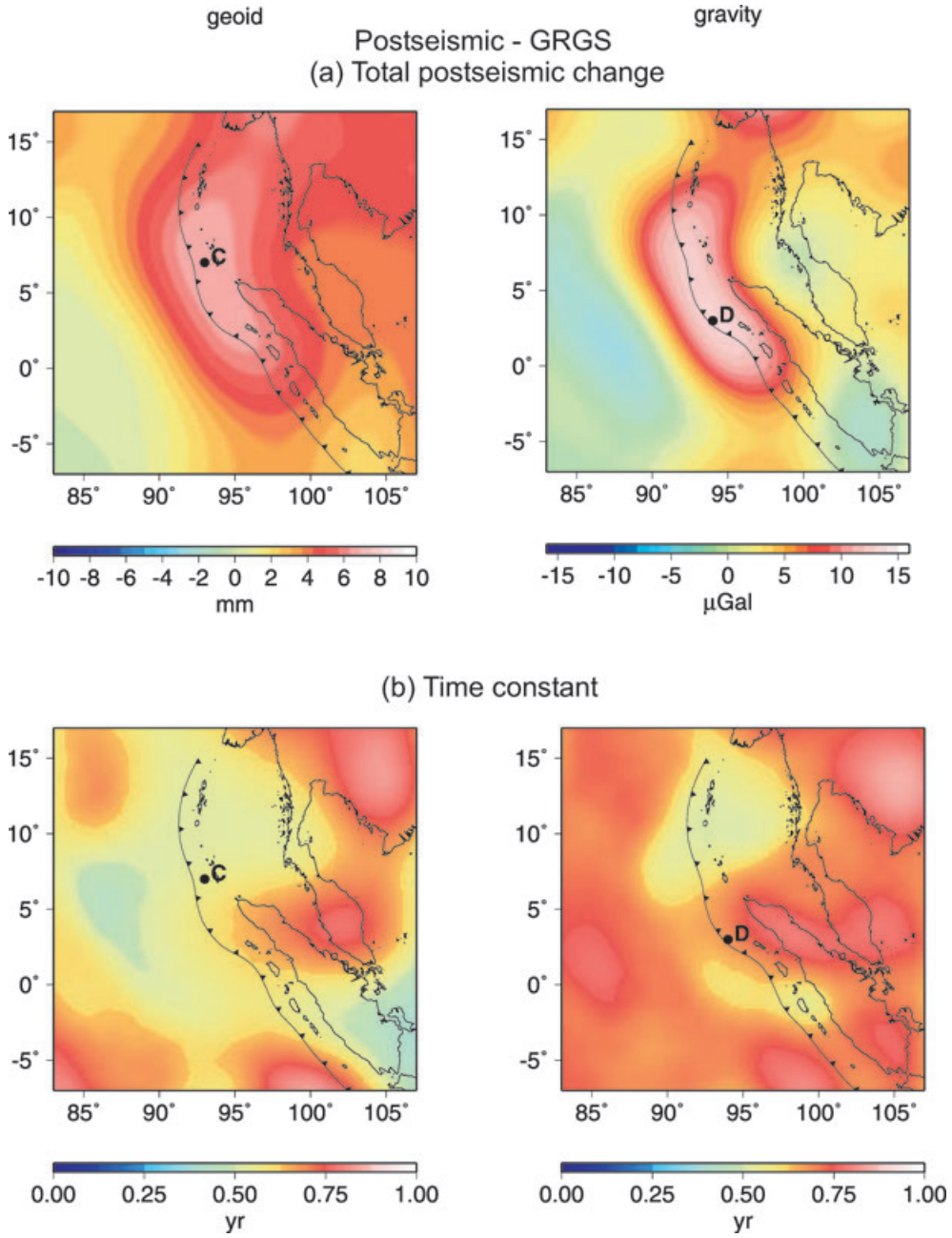


**Figure 6.** Total postseismic change (a) and time constant (b) of the postseismic relaxation affecting the geoid (left-hand panels) and the gravity (right-hand panels) estimated from the GRGS solutions. Black dots and associated letters indicate the locations where the time-series of Fig. 1 are plotted.

considering the uncorrected interannual variations from continental hydrology and oceanic circulation.

In the subduction zone, the annual wave is less than 3 μGal in both the models and GRACE. The annual signal in the Mekong basin is smaller in the models (maximal amplitude of 6 μGal) than in GRACE (maximal amplitude of 9 μGal). The ECCO analyses lead to a 7-μGal annual signal in the Gulf of Thailand, which is not detected by GRACE. In the preseismic linear trend, there is much more variability and larger amplitudes in GRACE than in the models. In GRACE, we find negative velocities around $-2$ μGal yr$^{-1}$ in a north–south stripe spreading on longitudes 95°E–100°E. On the contrary, the model velocities are zero in that area. Large negative velocities over Southeast Asia in GRACE agree well with the model velocities, in both combinations, over Myanmar only ($-1.5$ μGal yr$^{-1}$ in the models against $-2.4$ μGal yr$^{-1}$ in GRACE).

The total postseismic gravity change computed from the models (Fig. 11b) ranges between $-1$ and 2 μGal over the subduction area and in the Indian Ocean. This is comparable to the 1.2-μGal error associated to our estimated total postseismic gravity change in GRACE. So, the positive part of the postseismic signal observed in GRACE has no hydrological or oceanic origin. In the ECMWF + ECCO combination, the largest signal reaches 7 μGal in Malaysia and Gulf of Thailand. In the GLDAS + ECCO combination, the postseismic signal is clearly located offshore, in the Gulf of Thailand, reaching 6 μGal. South of Phuket, a 3-μGal signal is found in both model combinations. Consequently, the estimated postseismic gravity decrease of $-0.4 \pm 1.2$ μGal at 7°N–99°E (right-hand

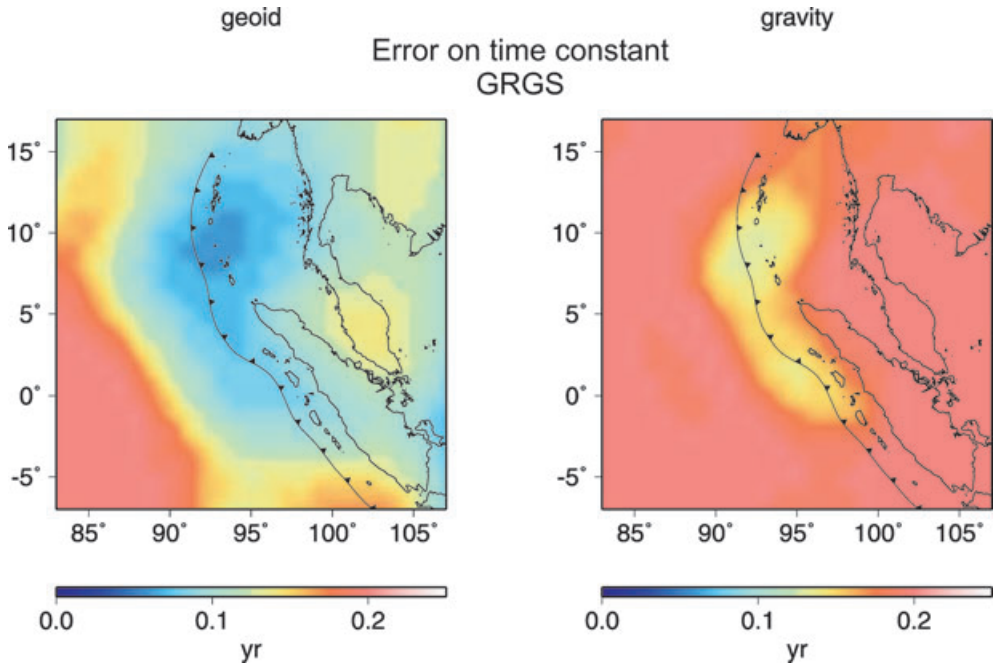


**Figure 7.** *A posteriori* error on the time constant of the postseismic relaxation affecting the geoid (left-hand panel) and the gravity (right-hand panel) estimated from the GRGS solutions.

panel of Fig. 6a) may have been underestimated by several μGals because of interannual hydrological and oceanic variations. The real postseismic gravity change may consist of a main central positive anomaly surrounded by two smaller negative ones of equal amplitudes.

Finally, the coseismic jump shown in Fig. 11(a) represents the error in our estimate of the coseismic effect since the models contain no jump. We do not find any significant signal over the subduction area nor in the Indian Ocean where values are overall slightly negative. In both combinations, we find a gradient from east to west. Minimal values reach −4 μGal in the Gulf of Thailand which is above the 1.5-μGal error on the estimated coseismic jump in GRACE in that area. However, no coseismic signal is found there. Therefore, the estimated negative coseismic anomaly in the eastern part of the Andaman Sea (Fig. 4a) may have been overestimated by 1–2 μGal because of a signal of hydrological and oceanic origin. Such a signal may also contribute by 2–3 μGal to the leakage of the GRACE negative anomaly in the southeastward direction. However, estimates from global hydrological models and an ocean circulation model cannot totally explain the strong negative anomaly in the Andaman Sea.

## 4 MODELLING OF COSEISMIC EFFECT IN GRAVITY FIELD

### 4.1 Theory

To compute the elasto-gravitational response of the Earth, we first compute the potential perturbation and deformation of the solid Earth and then the potential perturbation due to the ocean mass redistribution.

#### *4.1.1 Potential perturbation and deformation of the solid Earth*

To compute the static potential perturbation of the Earth, we sum the normal modes of an elastic, self-gravitating, non-rotating, spherical Earth generated by the earthquake (Saito 1967; Gilbert 1971). Gross & Chao (2006) use the same method to compute the effect of the Sumatra–Andaman earthquake on the length-of-day, polar motion and low-degree coefficients of the Earth's gravity field. An alternative approach to the static deformation consists in computing static dislocation Love numbers (Sun & Okubo 1993). Both calculations must provide the same results for a given earth model.

The gravitational potential perturbation $\Delta\Phi(r,\theta,\phi)$ induced by an internal point source located at $x_s$ with seismic moment $M_{ij}$ can be written as (Gilbert 1971; Aki & Richards 2002)

$$\Delta\Phi(r,\ \theta,\ \phi) = \sum_{n\ell m} \frac{M_{ij} : \varepsilon_{ij}^{\star(n\ell m)}(x_s)}{{}_n\omega_\ell^2}\, {}_nP_\ell(r) Y_{\ell m}(\theta,\ \phi), \qquad (4)$$

where $\varepsilon^{\star(n\ell m)}(x_s)$ is the complex conjugate of the strain generated by the $n\ell m$ mode at the source location and ${}_n\omega_\ell$ is the eigenfrequency of the mode. $n$ stands for the radial overtone number, $\ell$ is the spherical-harmonic degree and $m$ is the azimuthal order. ${}_nP_\ell(r)$ is the radial eigenfunction of the perturbation of the gravitational potential associated to the $n\ell m$ mode. $Y_{\ell m}(\theta,\phi)$ are the complex fully normalized spherical harmonics. By replacing ${}_nP_\ell$ by ${}_nU_\ell$, which is the radial eigenfunction of the vertical displacement of the $n\ell m$ mode, one obtains a similar expression for the vertical displacement $u_r(r,\theta,\phi)$.

We use the computer program MINOS based on a method developed by Woodhouse (1988) to compute the eigenfrequencies and eigenfunctions of the modes. We consider the anisotropic version of the PREM model (Dziewonski & Anderson 1981). However, the surface ocean layer is not very well modelled in MINOS, as the equations implemented are not suitable for a fluid. Therefore, the ocean mass redistribution due to the earthquake is not estimated, leading to unrealistic predictions at the ocean surface. That is why we choose to compute the response of the solid Earth by removing the 3-km-thick ocean layer from the PREM model. The response of the ocean is then solved analytically, as explained in Section 4.1.2

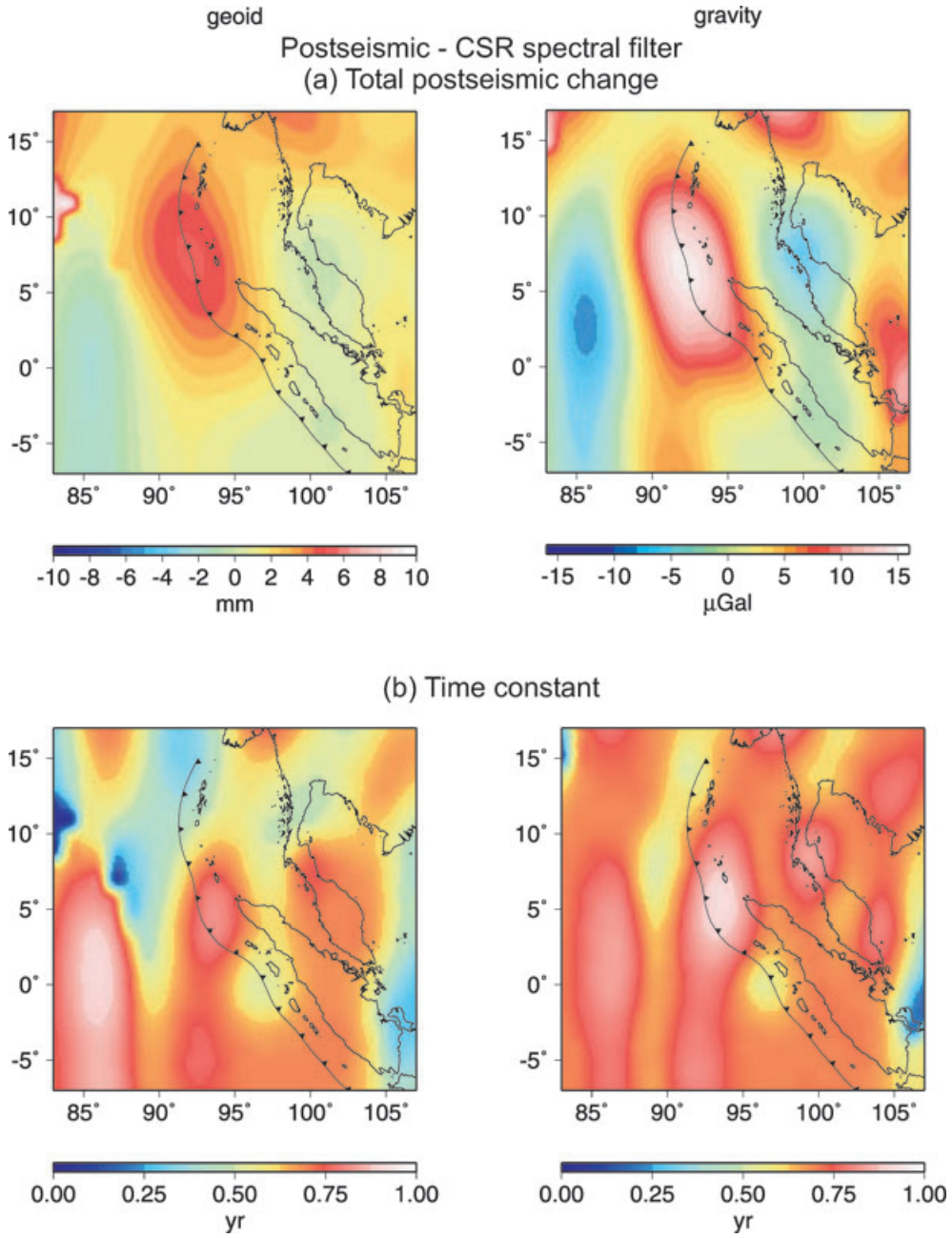


**Figure 8.** Total postseismic gravity change (a) and time constant (b) of the postseismic relaxation affecting the geoid (left-hand panels) and the gravity (right-hand panels) from the CSR-RL04 solutions after spectral filtering with a cosine taper over degrees $\ell = 30$–$50$.

Once the perturbation of the gravitational potential is known, it is straightforward to compute the displacement of the equipotential surface $\Delta N$ and variation of gravity $\Delta g$ at the surface of the crust $b = 6368$ km:

$$\Delta N(b,\,\theta,\,\phi) = -\frac{\Delta\Phi(b,\,\theta,\,\phi)}{g_0(b)}, \tag{5}$$

$$\Delta g(b,\,\theta,\,\phi) = \Delta\dot{\Phi}(b,\,\theta,\,\phi), \tag{6}$$

where $g_0(b)$ is the unperturbed gravity at $r = b$ and the dot denotes the radial derivative. The gravity variation at $r = b^+$ is given as a function of the vertical displacement $u_r(b,\theta,\phi)$ and the gravity variation at the top of the crust $r = b^-$ by

$$\Delta g(b^+,\,\theta,\,\phi) = \Delta g(b^-,\,\theta,\,\phi) + 4\pi G\Delta\rho(b)\,u_r(b,\,\theta,\,\phi). \tag{7}$$

$\Delta\rho(b)$ is the density contrast at the surface of our modified earth model, that is the density of the crust at $r = b$.

The potential and gravity perturbations are then continued upward to $a = 6378$ km where the GRACE solutions are computed.

Our approach is more realistic than that of Han *et al.* (2006) and Ogawa & Heki (2007). These authors first compute the displacement field and the subsequent volume strain caused by a finite dislocation in a homogeneous half-space. Next, they introduce a density discontinuity at the Moho depth and at the ocean bottom to compute the induced gravity changes.

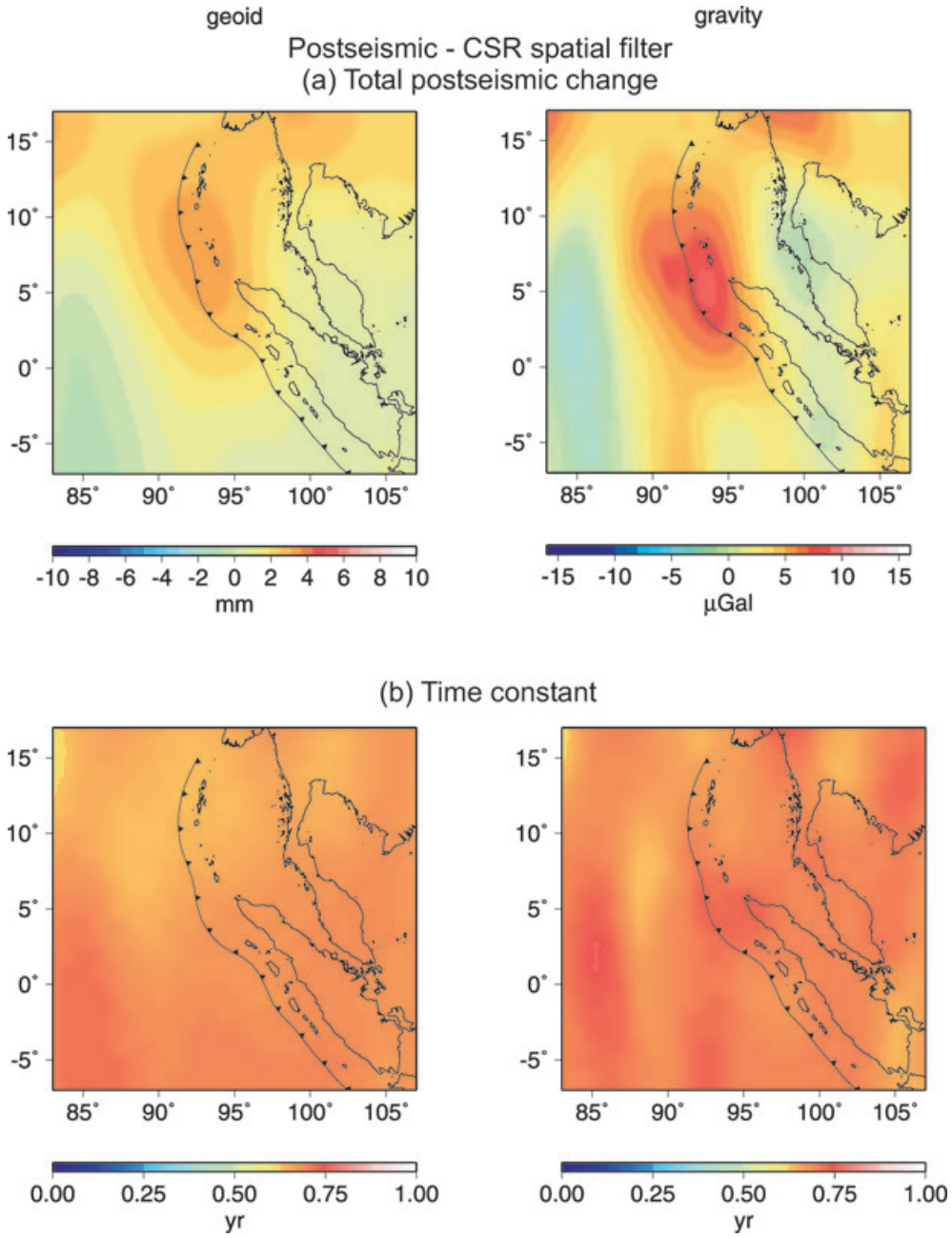


**Figure 9.** Total postseismic gravity change (a) and time constant (b) of the postseismic relaxation affecting the geoid (left-hand panels) and the gravity (right-hand panels) from the CSR-RL04 solutions after smoothing with a 350-km Gaussian filter.

#### *4.1.2 Potential perturbation of the ocean*

We compute the static potential perturbation of a global incompressible 3-km-thick ocean by imposing at its bottom the displacement field $u_r(b,\theta,\phi)$ and potential perturbation $\Delta\Phi(b,\theta,\phi)$ computed in Section 4.1.1. If we denote $\Delta P$ the total static perturbation of the gravity potential in the ocean, the displacement of the equipotential surface $\Delta N$ at the surface of the ocean $c = 6371$ km, that is, the displacement of the geoid, and the gravity perturbation $\Delta g$ are

$$\Delta N(c,\,\theta,\,\phi) = -\frac{\Delta P(c,\,\theta,\,\phi)}{g_0(c)}, \tag{8}$$

$$\Delta g(c,\,\theta,\,\phi) = \Delta \dot{P}(c,\,\theta,\,\phi)\,. \tag{9}$$

The degree-$\ell$ term of $\Delta P$ is given by

$$\Delta P_\ell(c) = \frac{1}{\frac{(2\ell+1)\,g_0(c)}{4\pi G\rho_w c} - 1}\left(\frac{b}{c}\right)^{\ell+1}\left[\Delta\Phi_\ell(b) + \frac{b}{c}g_0(b)\,u_{r,\,\ell}(b)\right], \tag{10}$$

where $\rho_w$ is the density of the ocean. $\Delta N$ and $\Delta g$ at $r = c$ are then continued upwards to $r = a$. The degree-$\ell$ term of $\Delta g$ is found by derivating eq. (10):

$$\Delta g_\ell(c) = -(\ell+1)\frac{\Delta P_\ell(c)}{c}\,. \tag{11}$$

The deformed ocean loads the solid Earth, whose subsequent deformation is responsible for a secondary effect on the ocean. A straightforward calculation of the secondary deformation of

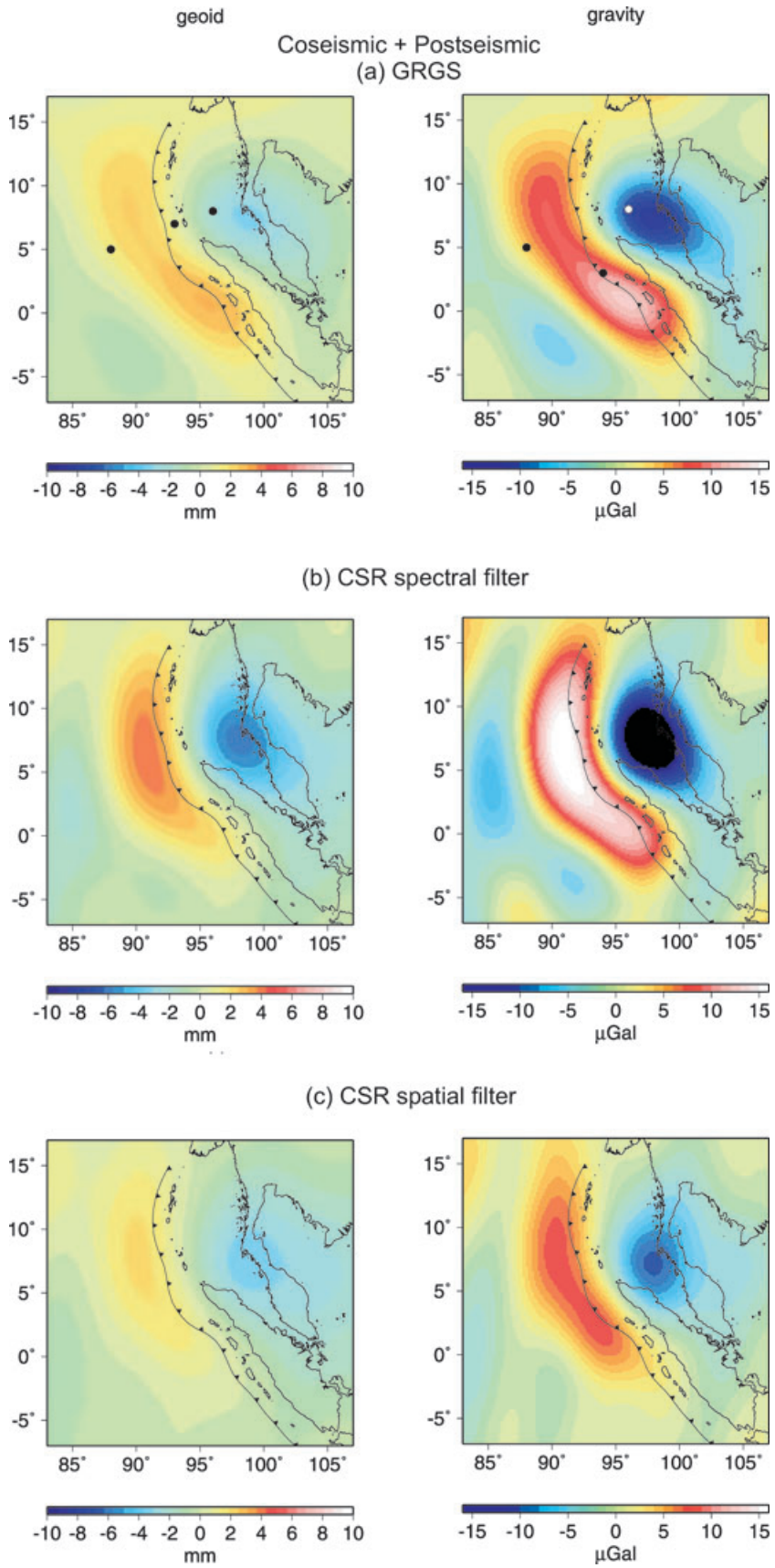


**Figure 10.** Permanent effect (coseismic + postseismic) 26 months after the earthquake affecting the geoid (left-hand panel) and the gravity (right-hand panel) from the GRACE gravity fields of GRGS (a) and CSR after a spectral filtering with a cosine taper over degrees $\ell$ = 30–50 (b) or a smoothing with a 350-km Gaussian filter (c).

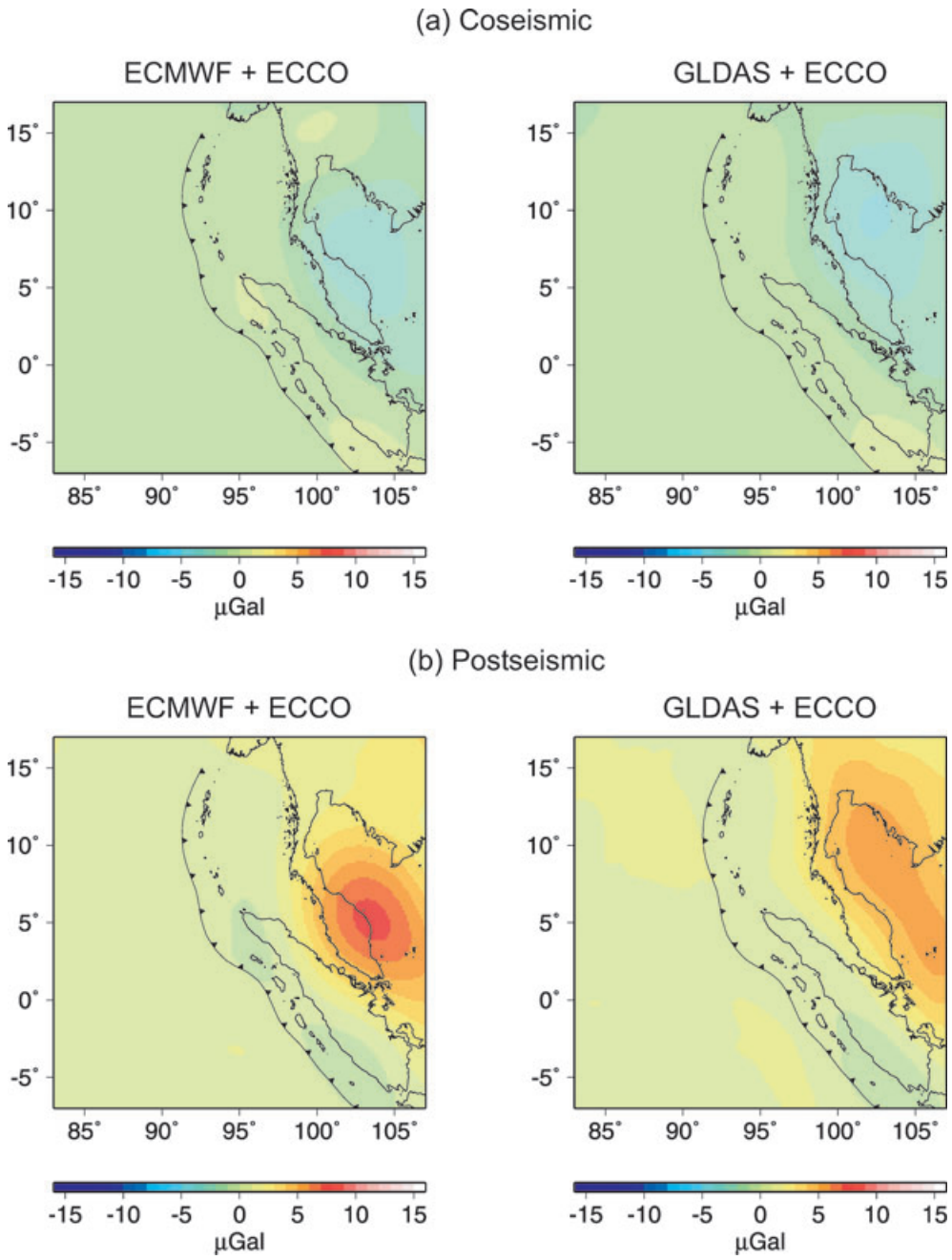


**Figure 11.** Impact of global hydrology and oceanic circulation on the GRACE estimates of the coseismic and postseismic gravity changes. Estimated contribution on the coseismic jump (a) and total postseismic gravity change (b) from the ECMWF + ECCO (left-hand panels) and GLDAS + ECCO (right-hand panels) model combinations.

the ocean however shows that it is one order of magnitude smaller than the primary effect and consequently we neglect it.

The total response at $r = a$ is then the sum of the upward continued effects given by eqs (5) and (8) for the potential perturbation, and eqs (6) and (9) for the gravity perturbation:

$$\Delta N(a,\,\theta,\,\phi) = -\frac{\Delta\Phi(a,\,\theta,\,\phi) + \Delta P(a,\,\theta,\,\phi)}{g_0(a)}, \tag{12}$$

$$\Delta g(a,\,\theta,\,\phi) = \Delta\dot{\Phi}(a,\,\theta,\,\phi) + \Delta\dot{P}(a,\,\theta,\,\phi)\,. \tag{13}$$

### 4.2 Numerics

For each harmonic degree $\ell$, we sum over all the overtones with eigenfrequency smaller than 120 mHz to achieve the convergence of the series given by eq. (4). We start the sum over the spherical-harmonic degree at $\ell = 2$. To get a similar spectral content as GRACE observations, we low-pass filter the eigenfunctions in the spectral domain with a cosine taper decreasing from one at $\ell = 30$ to zero at $\ell = 50$.

For each observable $N$, $g$ and $u_r$, we compute the cumulative effect of all the point sources of the seismic moment distribution on

a 24° × 24° area gridded at a 5-km interval. We use the Ammon *et al.* (2005) source model. The fault rupture of about 1200 × 200 km is represented by 850 point dislocations equally distributed with variable dislocation and slip orientation. These authors chose the strike and dip of the individual sources according to the subduction geometry and inverted the rake and slip from seismological data: body and surface waves as well as normal modes. The total seismic moment is $9 \times 10^{22}$ N m.

### 4.3 Results

The modelled coseismic displacement of the equipotential surface $\Delta N$ and gravity variation $\Delta g$ are plotted in Fig. 12.

The response of the solid Earth, given by eqs (5) and (6), is shown in Fig. 12(a). It consists in a dipole whose negative anomaly reaches −2.8 mm for the geoid and −12 μGal for the gravity and positive anomaly reaches 3.3 mm for the geoid and 14 μGal for the gravity. The negative anomaly is centred in the southeastern part of the Andaman Sea. Its absolute amplitude is slightly smaller than the positive anomaly that lies west of the trench. This solid Earth contribution does not correlate very well with the GRACE observations.

The response of the ocean, given by eqs (8) and (9), is plotted in Fig. 12(b). It consists in a quasi-spherical negative anomaly centred over the trench offshore, between the Nicobar Islands and the northern tip of Sumatra. It reaches −4.0 mm for the geoid and −11 μGal for the gravity.

Finally, the sum of both contributions is plotted in Fig. 12(c). The signature is still dipolar but the negative anomaly is dominant. Consequently, the average over the area is negative. The peak-to-peak amplitude is 4.6 mm for the geoid and 20 μGal for the gravity. The positive anomaly is located west of the trench and centred at 2–3°N–92°E. In gravity, it follows the trench remarkably well along its eastern side. The maximum amplitude is 0.1 mm for the geoid and 5.4 μGal for the gravity. The negative anomaly is located in the southern part of the Andaman Sea and centred at 8°N–97°E. It reaches −4.5 mm for the geoid and −14.3 μGal for the gravity.

The GRACE estimate of Fig. 4 and the seismic model of Fig. 12 agree well regarding the gravity change and quite well for the geoid displacement. In particular, we succeed in restituting the main characteristics of the observed coseismic signature, such as the overall shape, the order of magnitude of the peak-to-peak amplitudes, the large weight of the negative anomaly as well as its location. However, the modelled positive anomaly is located between the two positive anomalies observed in GRACE. On the contrary to the model, the observed negative anomaly leeks southeastwards, over the Malay Peninsula and the Gulf of Thailand. This difference has been mainly explained in Section 3 by the effect of interannual variations in the ocean circulation over the Gulf of Thailand. Regarding the gravity change, the model extrema are −14.3 and +5.4 μGal. The peak-to-peak amplitude is the same as the GRACE estimate but the model extrema are 2 μGal larger than the observed ones. This discrepancy is not significant when compared to the 1.5-μGal error on the coseismic estimate. The peak-to-peak amplitude of the modelled geoid variation is 2 mm smaller than in the GRACE observations. The maximum value over the area is +0.1 mm in the model whereas it is −1 mm in the GRACE observations. The modelled negative anomaly reaches −4.5 mm. It is not as large as the −8 mm of observed geoid decrease. As for the gravity variation, we can show from global model outputs that there is almost no contamination from ocean circulation nor continental hydrology in the Andaman Sea. So, the discrepancy between the model and the observation is likely to the effect of a source located in the solid Earth.

Panet *et al.* (2007) partly explained such a discrepancy by a 15-cm additional subsidence of the seafloor in the Andaman Sea due to a less rigid regional lithosphere. Nevertheless, in a full-resolution geoid, the negative anomaly should be located westwards, right above the subduction zone. Then, the effect of the filtering is to move the anomaly eastwards, in the Andaman Sea. So, the geophysical origin of such strong negative anomaly is probably not located in the Andaman Sea but may be due to stronger ground displacements above the down-dip end of the slab.

## 5 COMPARISON WITH PREVIOUS STUDIES AND DISCUSSION

### 5.1 Coseismic effect

Our GRACE estimate of the effect on the geoid is less negative west of the trench than the 2005 January minus 2004 January difference computed by Panet *et al.* (2007) for the same GRGS solutions. In the Andaman Sea, the amplitudes are similar. We can only qualitatively compare our results with their wavelet analysis of the effect on the geoid that provides correlation coefficients: our estimate of the effect on the geoid is very similar to their 1000-km scale wavelet analysis and our estimate of the effect on the gravity agrees well with their 570-km scale wavelet analysis although, in this case, they find a smaller positive anomaly compared to the negative anomaly.

Also, our estimate of the effect on the geoid agrees also well in shape and amplitude with that of Ogawa & Heki (2007), although they use solutions smoothed with a 350-km Gaussian filter (Table 1).

Han *et al.* (2006) and Chen *et al.* (2007) find a stronger positive gravity anomaly located further south than ours. This difference is not found anymore in the recent work of Han & Simons (2008). In Chen *et al.* (2007), Han *et al.* (2006) and Han & Simons (2008), the peak-to-peak amplitude is larger, about 30 μGal. For the last two studies, this may be explained by the higher spatial resolution of the gravity solutions. Besides, as Chen *et al.* (2007) and Han *et al.* (2006) stacked annual differences over 6 and 21 months, respectively, their coseismic signature is contaminated by the postseismic effect and is similar to our estimate of the permanent effect, in particular for Chen *et al.* (2007) whose stacking period is the longest.

Our modelled coseismic gravity change is quite similar to that of Han *et al.* (2006) although they use a different modelling and filtering strategy (Table 1). They find a larger peak-to-peak amplitude (about 30 μGal) and their negative anomaly does not seem to be as large with respect to the positive one as in our model. Ogawa & Heki (2007) find a similar pattern of amplitudes for the geoid, but, once again, with a 3-mm larger negative anomaly after a spatial smoothing. They explain the stronger negative anomaly by dilatation in the crust. In our study, this contribution is present but we do not isolate this effect. However, our modelled total response of the solid Earth without ocean does not correlate with the GRACE observations. We show in Section 4 that the effect of the ocean mass redistribution must be added to explain the observed overall negative signature. This effect is, however, neglected by Han *et al.* (2006) and Ogawa & Heki (2007).

### 5.2 Postseismic effect

Our estimate of the postseismic signature 26 months after the earthquake from the GRACE observations is better constrained from

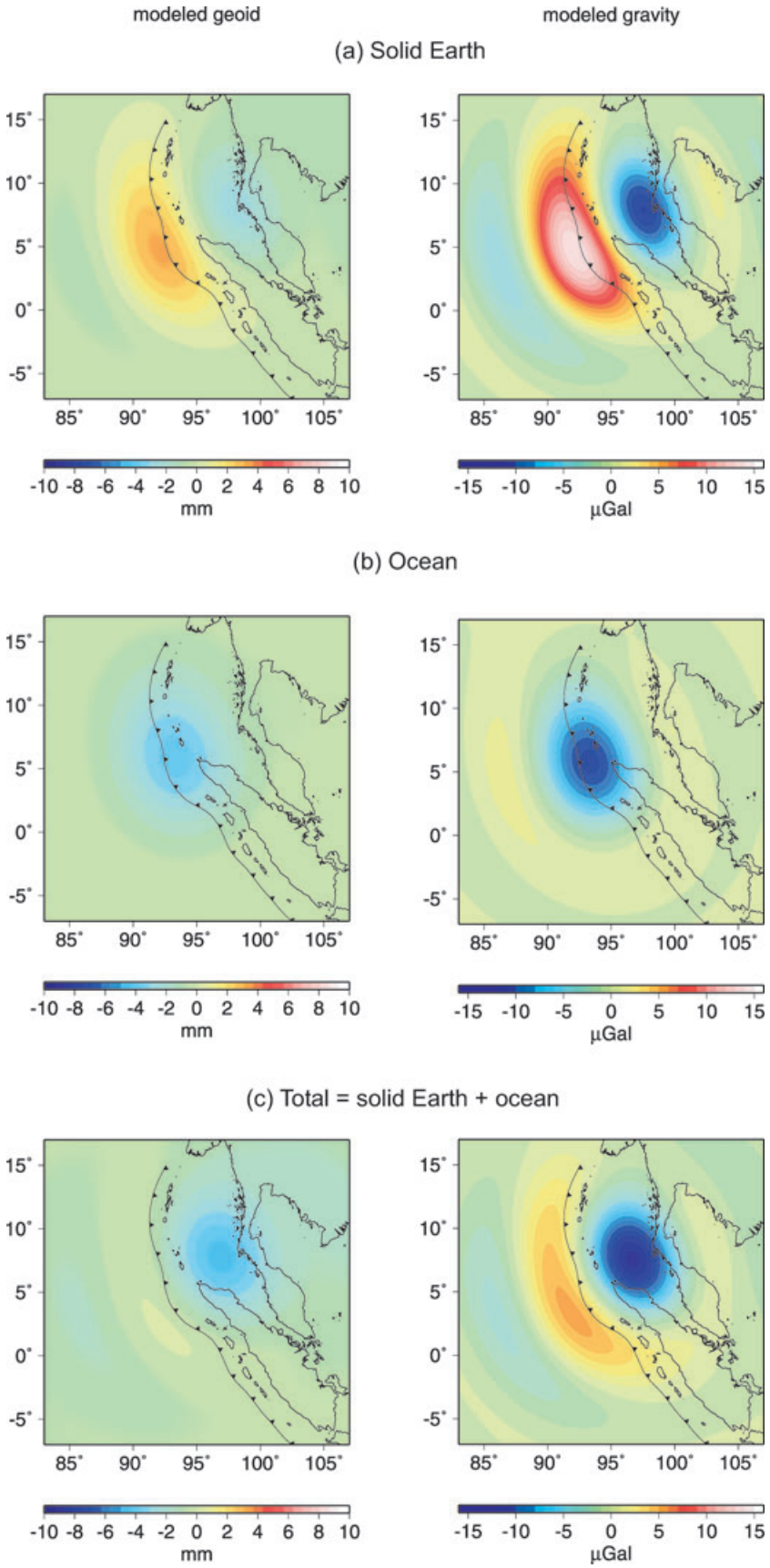


**Figure 12.** Modelled coseismic jump affecting the geoid (left-hand panel) and the gravity (right-hand panel) after spectral filtering with a cosine taper over degrees $\ell = 30$–$50$. The complete signature (c) is obtained from the contribution of the solid Earth (a) and the subsequent ocean mass redistribution (b).

the GRGS solutions than from the CSR-RL04 solutions for both parameters that characterize the relaxation. It consists in a 'banana-shaped' positive anomaly centred on the Sunda trench spreading over 15° of latitude from south of the epicentre to the Andaman Islands. The amplitude of 6.8 mm in the geoid variation is comparable to that of Ogawa & Heki (2007), although they use different solutions that are smoothed with a 350-km Gaussian filter and disturbed by north–south stripes. Regarding the effect on the geoid, the relaxation time is about $0.6 \pm 0.07$ yr, indicating a very good spatial correlation of the process at large scale. At a smaller scale, for the gravity variation, relaxation is a bit slower ($\tau = 0.7 \pm 0.15$ yr) on an area lying between 0°N and 6°N. However, these spatial heterogeneities of the relaxation time are too small to be sensibly interpreted as spatial heterogeneities of the mantle or lower crust viscosity.

We do not find any postseismic signal initiated in the Andaman Sea as mentioned in Panet *et al.* (2007) that would give a relaxation time smaller in the Andaman Sea than above the trench. On the contrary, we detect a 161-d signal due to the $S_2$ aliasing whose maximum is located in the Andaman Sea. Because this signal is in an ascending phase within the 2–3 months following the earthquake, as shown by the bottom centre panel of Fig. 1, it may have been erroneously interpreted as a transient postseismic signal.

Vertical deformation measurements by GPS and remote sensing (Synthetic Aperture Radar, optical imagery) or *in situ* biological observations of coral reefs can be compared with the postseismic signature seen by GRACE, in particular their temporal evolution. Because there are no ocean bottom observations and only very few land observations, it is difficult to compare the spatial distributions of both observables. In addition, near-field terrestrial observations have a much better spatial resolution than satellite gravity data. Kayanne *et al.* (2007) made measurements of biological indicators up to 1 yr after the earthquake. They report a postseismic subsidence following the coseismic uplift and occurring within 2 months after the earthquake at Mayabunder, in Middle Andaman Island. On the opposite, uplift was measured by GPS at Port Blair, in South Andaman Island over a 12-d period in 2005 January (Gahalaut *et al.* 2006). This positive trend has been going on for 2 yr at each of the eight observation sites measured by GPS in the Andaman Islands (Paul *et al.* 2007). Their 0.82-yr relaxation time inverted from both the horizontal and vertical ground displacements of all sites is of the same order as our estimate from the satellite gravity data. However, more observations would be needed, in particular in the far field (such as in Thailand, Indonesia and Malaysia), to get the large-scale component of vertical displacement. Rapid postseismic afterslip is reported by different authors up to 50 d after the earthquake in the horizontal components (Vigny *et al.* 2005; Gahalaut *et al.* 2006).

Different geophysical explanations are put forward to explain the observed postseismic ground motions and gravity changes: afterslip, viscoelastic relaxation and poroelastic rebound.

Paul *et al.* (2007) show that afterslip best explains the full vector of observed ground motions at some sites in the Andaman Islands, in particular the relaxation time. They build a postseismic slip model in that region showing slip located on the down-dip end of the coseismic rupture area. However, an afterslip model for a larger region would be necessary to compute the corresponding effect in gravity and compare it with GRACE as Chlieh *et al.* (2007) did for the first month after the earthquake. They found that the postseismic moment release by afterslip equaled on average 35 per cent of the coseismic moment, and could even be larger than 100 per cent in the vicinity of the Andaman Islands.

Pollitz *et al.* (2006) modelled the observed GPS horizontal motions between the 2004 December 26 and the 2005 March 28 earthquakes. They use a spherically layered compressible earth model with a biviscous rheology for the asthenosphere. The transient viscosity of $5 \times 10^{17}$ Pa s is responsible for the short relaxation time of 0.23 yr. Only the vertical component in Phuket (Thailand) is discussed: model and observations agree quite well despite of noisy data. The pattern of their predicted vertical velocity 3 months after the earthquake agrees very well with our 'banana-shaped' GRACE estimate of the postseismic gravity change 26 months after the earthquake. Indeed, we can assume that the spatial patterns of predicted vertical velocity are similar 3 and 26 months after the earthquake, except that the amplitudes must be larger after 26 months. Assuming no response of the ocean, the pattern in the gravity field may also be similar to that in the vertical velocity field. Moreover, the spatial pattern of the postseismic relaxation predicted by Pollitz *et al.* (2006) is a large-scale signal contrary to the coseismic effect that reflects the small wavelengths of the seismic source. Therefore, the effect of the GRACE limited bandwidth may be less drastic for the postseismic effect. GRACE is likely to bring a more complete information on the postseismic effect than on the coseismic one.

Tanaka (personal communication, 2007) computed the postseismic geoid height variation for a spherically layered compressible earth model with a 50-km purely elastic crust above a mantle with a Maxwell rheology of constant viscosity (Tanaka *et al.* 2006). A small value of $10^{18}$ Pa s for the viscosity was needed to fit the 2-yr mean of the observed geoid change. However, a longer time-series has to be used to better determine the long-term relaxation velocity in GRACE.

Finally, Ogawa & Heki (2007) provide evidence for poroelastic rebound caused by water mantle diffusion from a compressed area to a depressed one at the down-dip end of the earthquake rupture zone.

## 6 CONCLUSION

We have carried out a space-based inversion of the time-variable gravity field solutions at about 600 km spatial resolution estimated from the GRACE observations to carefully split the effects of various geophysical sources: coseismic effect; postseismic relaxation; seasonal-to-interannual variations from continental hydrology and ocean circulation and aliasing errors of high-frequency sources that appear as long-period signals. Our estimates of the coseismic and postseismic signatures are consequently not correlated from each other nor biased by effects of other geophysical sources. Although the signal-to-noise ratio as well as the signal amplitudes depend on the filtering strategy of the GRACE solutions, a clear negative gravity drop is systematically estimated east of the Sunda trench dominating the coseismic signature, while a more discreet positive anomaly lies west of the trench. The complete modelling of the coseismic gravity effect using a stratified, spherically symmetric earth model, as well as a more realistic response of the ocean, allows us to maintain that crustal dilatation is not the main cause of the observed strong gravity decrease. Instead, we show that the effect of the ocean mass lateral redistribution that is neglected in previous studies is far to be negligible. Taking this contribution into account leads to a much better correlation with the GRACE observation, in particular at small scales, around 600 km.

The postseismic signature estimated 26 months after the earthquake consists in a large-scale gravity increase centred above the trench and extending over 15° of latitude along the subduction. Two

symmetric negative anomalies are located at the western and eastern sides of the main anomaly. Although the relaxation time is better constrained by the GRGS solutions than by the CSR ones, spatial variations of this parameter around the 0.7 yr mean value cannot be interpreted as spatial heterogeneities in the mantle. Moreover, among the three geophysical processes invoked to explain postseismic deformation (afterslip, viscous relaxation and poroelastic rebound), it is likely that all occur simultaneously. Further investigation on the separation of the above phenomena in the GRACE time-variable gravity field solutions may be done to better constrain geophysical models. Longer postseismic period may also help to better constrain the upper-mantle rheology.

## ACKNOWLEDGMENTS

We are grateful to Jean-Michel Lemoine and Sylvain Loyer for fruitful discussions and for providing us the GRGS solutions. We thank Chen Ji for providing us his seismic source model for the Sumatra–Andaman earthquake. We furthermore wish to acknowledge Yoshiyuki Tanaka for computing the coseismic and postseismic gravity changes using the dislocation Love numbers. We are grateful to Isabelle Panet for kindly answering our questions. Finally, two anonymous reviewers helped to improve the manuscript.

## REFERENCES

Aki, K. & Richards, P.G., 2002. *Quantitative Seismology,* 2nd edn, Freeman, New York.

Ammon, C.J. *et al*., 2005. Rupture process of the 2004 Sumatra-Andaman earthquake, *Science,* **308,** 1133–1139.

Bettadpur, S., 2007. *Gravity Recovery and Climate Experiment Level-2 Gravity Field Product User Handbook,* Rev. 2.3, Center for Space Research, The University of Texas at Austin.

Biancale, R. *et al*., 2008. 6 years of gravity variations from GRACE and LAGEOS data at 10-day intervals over the period from July 29th, 2002 to May 27th, 2008, available at http://bgi.cnes.fr:8110/geoid-variations/README.html.

Chen, J.L., Wilson, C.R., Tapley, B.D. & Grand, S., 2007. GRACE detects coseismic and postseismic deformation from the Sumatra-Andaman earthquake, *Geophys. Res. Lett.,* **34,** L13302, doi:10.1029/2007GL030356.

Cheng, M. & Tapley, B.D., 2004. Variations in the Earth's oblateness during the past 28 years, *J. geophys. Res.,* **109,** B09402, doi:10.1029/2004JB003028.

Chlieh, M. *et al*., 2007. Coseismic slip & afterslip of the Great Mw 9.15 Sumatra-Andaman Earthquake of 2004, *Bull. seism. Soc. Am.,* **97**(1A), S152–S173.

Dziewonski, A. & Anderson, D.L., 1981. Preliminary Reference Earth Model, *Phys. Earth planet. Inter.,* **25,** 297–356.

Flechtner, F., 2007. *AOD1B Product Description Document for Product Releases 01 to 04, GRACE 327-750 (GR-GFZ-AOD-0001),* Rev. 3.1, GeoForschungZentrum, Potsdam.

Frappart, F., Do Minh, K., L´Hermitte, J., Cazenave, A., Ramillien, G., Le Toan, T. & Mognard-Campbell, N., 2006. Water volume change in the lower Mekong from satellite altimetry and imagery data, *Geophys. J. Int.,* **167,** 570–584.

Freymueller, J.T., Cohen, S.C. & Fletcher, H.J., 2000. Spatial variations in present-day deformation, Kenai Peninsula, Alaska, and their implications, *J. geophys. Res.,* **105**(B4), 8079–8102.

Gahalaut, V.K., Nagarajan, B., Catherine, J.K. & Kumar, S., 2006. Constraints on 2004 Sumatra-Andaman earthquake rupture from GPS measurements in Andaman-Nicobar Islands, *Earth planet. Sci. Lett.,* **242,** 365–374.

Gilbert, F., 1971. Excitation of the normal modes of the Earth by earthquakes, *Geophys. J. R. astr. Soc.,* **22,** 223–226.

Gross, R.S. & Chao, B.F., 2006. The rotational and gravitational signature of the December 26, 2004 Sumatran earthquake, *Surv. Geophys.,* **27,** 615–632.

Gudmundsson, O. & Sambridge, M., 1998. A regionalized upper mantle (RUM) seismic model, *J. geophys. Res.,* **103,** 7121–7136.

Han, S.-C. & Simons, F.J., 2008. Spatiospectral localization of global geopotential fields from the Gravity Recovery and Climate Experiment (GRACE) reveals the coseismic gravity change owing to the 2004 Sumatra-Andaman earthquake, *J. geophys. Res.,* **113,** B01405, doi:10.1029/2007JB00492710.1029/2007JB004927.

Han, S.-C., Shum, C.K., Bevis, M., Ji, C. & Kuo, C.-Y., 2006. Crustal dilatation observed by GRACE after the 2004 Sumatra-Andaman Earthquake, *Science,* **313,** 658–662.

Kayanne, H. *et al*., 2007. Coseismic and postseismic creep in the Andaman Islands associated with the 2004 Sumatra-Andaman earthquake, *Geophys. Res. Lett.,* **34,** L01310, doi:10.1029/2006GL028200.

Lemoine, J.-M., Bruinsma, S., Loyer, S., Biancale, R., Marty, J.-C., Perosanz, F. & Balmino, G., 2007. Temporal gravity field models inferred from GRACE data, *Adv. Space Res.,* **39,** 1620–1629.

Lyard, F., Lefèvre, F., Letellier, T. & Francis, O., 2006. Modelling the global ocean tides: modern insights from FES2004, *Ocean Dyn.,* **56**(5–6), 394–415.

Mikhailov, V., Tikhotsky, S., Diament, M., Panet, I. & Ballu, V., 2004. Can tectonic processes be recovered from new gravity satellite data?, *Earth planet. Sci. Lett.,* **228,** 281–297.

Montesi, L.G.J., 2004. Controls of shear zone rheology and tectonic loading on postseismic creep, *J. geophys. Res.,* **109,** B10404, doi:10.1029/2003JB002925.

Ogawa, R. & Heki, K., 2007. Slow postseismic recovery of geoid depression formed by the 2004 Sumatra-Andaman Earthquake by mantle water diffusion, *Geophys. Res. Lett.,* **34,** L06313, doi:10.1029/2007GL029340.

Panet, I. *et al*., 2007. Coseismic and post-seismic signatures of the Sumatra 2004 December and 2005 March earthquakes in GRACE satellite gravity, *Geophys. J. Int.,* **171,** 177–190.

Paul, J., Lowry, A.R., Bilham, R., Sen, S. & Smalley, R.J., 2007. Coseismic and postseismic creep in the Andaman Islands associated with the 2004 Sumatra-Andaman earthquake, *Geophys. Res. Lett.,* **34,** L19309, doi:10.1029/2007GL03102410.1029/2007GL031024.

Peltzer, G., Rosen, P., Rogez, F. & Hudnut, K., 1998. Poroelastic rebound along the Landers 1992 earthquake surface rupture, *J. geophys. Res.,* **103**(B12), 30 131–30 145.

Pollitz, F.F., Bürgmann, R. & Banerjee, P., 2006. Post-seismic relaxation following the great 2004 Sumatra-Andaman earthquake on a compressible self-gravitating Earth, *Geophys. J. Int.,* **167,** 397–420.

Ray, R.D. & Luthcke, S.B., 2006. Tide model errors and GRACE gravimetry: towards a more realistic assessment, *Geophys. J. Int.,* **167,** 1055–1059.

Reigber, C., Schmidt, R., Flechtner, F., König, R., Meyer, U., Neumayer, K.-H., Schwintzer, P. & Zhu, S.Y., 2005. An Earth gravity field model complete to degree and order 150 from GRACE: EIGEN-GRACE02S, *J. Geodyn.,* **39,** 1–10.

Rodell, M. *et al*., 2004. The Global Land Data Assimilation System, *Bull. seism. Soc. Am.,* **85**(3), 381–394.

Saito, M., 1967. Excitation of free oscillations and surface waves by a point source in a vertically heterogeneous Earth, *J. geophys. Res.,* **72**(4), 3689–3699.

Schmidt, R. *et al*., 2006. GRACE observations of changes in continental water storage, *Global Planet. Change,* **50**(1–2), 112–126.

Stammer, D., Wunsch, C., Fukumori, I. & Marshall, J., 2002. State Estimation in Modern Oceanographic Research, *EOS, Trans. Am. geophys. Un.,* **83**(27), 289 &294–295.

Stein, S. & Okal, E.A., 2005. Speed and size of the Sumatra earthquake, *Nature,* **434,** 581–582.

Sun, W. & Okubo, S., 1993. Surface potential and gravity changes due to internal dislocations in a spherical Earth, I. Theory for a point dislocation, *Geophys. J. Int.,* **114,** 569–592.

Sun, W. & Okubo, S., 2004a. Coseismic deformations detectable by satellite gravity missions: a case study of Alaska (1964, 2002) and Hokkaido

(2003) earthquakes in the spectral domain, *J. geophys. Res.,* **109,** B04405, doi:10.1029/2003JB002554.

Sun, W. & Okubo, S., 2004b. Truncated co-seismic geoid and gravity changes in the domain of spherical harmonic degree, *Earth Planets Space,* **56,** 881–892.

Tanaka, Y., Okuno, J. & Okubo, S., 2006. A new method for the computation of global viscoelastic post-seismic deformation in a realistic earth model (I)–vertical displacement and gravity variation, *Geophys. J. Int.,* **164,** 273–289.

Tapley, B.D., Bettadpur, S., Ries, J.C., Thompson, P.F. & Watkins, M.M., 2004. GRACE measurements of mass variability in the Earth system, *Science,* **305,** 503–505.

Tarantola, A., 2005. *Inverse Problem Theory and Methods for Model Parameter Estimation,* Society for Industrial and Applied Mathematics, Philadelphia, Pennsylvania.

Vigny, C. *et al*., 2005. Insight into the 2004 Sumatra-Andaman earthquake from GPS measurements in southeast Asia, *Nature,* **436,** 201–206.

Viterbo, P. & Beljaars, A.C.M., 1995. An improved land surface parameterization scheme in the ECMWF model and its validation, *J. Clim.,* **8,** 2716–2748.

Wahr, J., Swenson, S., Zlotnicki, V. & Velicogna, I., 2004. Time-variable gravity from GRACE: first results, *Geophys. Res. Lett.,* **31,** L11501, doi:10.1029/2004GL019779.

Wahr, J., Swenson, S. & Velicogna, I., 2006. Accuracy of GRACE mass estimates, *Geophys. Res. Lett.,* **33,** L06401, doi:10.1029/2005GL025305.

Woodhouse, J.H., 1988. The calculation of eigenfrequencies and eigenfunctions of the free oscillations of the Earth and the Sun, in *Seismological Algorithms, Computational Methods and Computer Programs,* ed. Doornbos, D.J., Springer, New York.